YALE
PEABODY
MUSEUM

JOURNAL OF MARINE RESEARCH

The *Journal of Marine Research,* one of the oldest journals in American marine science, published important peer-reviewed original research on a broad array of topics in physical, biological, and chemical oceanography vital to the academic oceanographic community in the long and rich tradition of the Sears Foundation for Marine Research at Yale University.

An archive of all issues from 1937 to 2021 (Volume 1–79) are available through EliScholar, a digital platform for scholarly publishing provided by Yale University Library at https://elischolar.library.yale.edu/.

Requests for permission to clear rights for use of this content should be directed to the authors, their estates, or other representatives. The *Journal of Marine Research* has no contact information beyond the affiliations listed in the published articles. We ask that you provide attribution to the *Journal of Marine Research.*

Yale University provides access to these materials for educational and research purposes only. Copyright or other proprietary rights to content contained in this document may be held by individuals or entities other than, or in addition to, Yale University. You are solely responsible for determining the ownership of the copyright, and for obtaining permission for your intended use. Yale University makes no warranty that your distribution, reproduction, or other use of these materials will not infringe the rights of third parties.

Forced double Kelvin waves in a stratified ocean

by Andrew J. Willmott[1,2]

ABSTRACT

This paper examines the linear response of a two-layer uniformly rotating ocean of infinite horizontal extent with a discontinuity in depth to a divergence-free transient wind stress. Initially the ocean is at rest and the wind stress is directed perpendicular to the escarpment. A rigid lid is employed to filter out the external double Kelvin wave and an analytic solution is derived, using transform techniques, for the forced internal double Kelvin wave which is trapped along the depth discontinuity. Parameter values are chosen which most accurately model the Mendocino escarpment oriented almost zonally off the northern California coast.

Soon after the wind stress is applied a single large wave is generated in the neighborhood of the wind stress curl origin. The wave has a maximum amplitude of 3 m, a phase speed of approximately 2.2 km day^{-1} and a wavelength in the order of 200 km. Furthermore the forced double Kelvin wave is found to exhibit a 6 day oscillation which is independent of the *e*-folding time scale of the wind stress. At any fixed location along the escarpment the solution also displays amplitude modulation. An investigation of how sensitive the solutions are to the upper layer depth and stratification is presented. A brief discussion of the response produced by a time-periodic spatially independent wind stress directed parallel to the escarpment and suddenly applied to a quiescent ocean, is also presented. It is suggested that double Kelvin waves may perhaps be detected from deep-sea buoy measurements.

1. Introduction

Satellite infrared imagery off the California coast reveals the presence of thermal intrusions (perhaps thermal streamers is a better term) which originate in the coastal upwelling zone over the continental shelf and shelf break. These cold water intrusions can have an offshore scale of the order of 500 km and they frequently appear to originate from the vicinity of coastal capes, where upwelling is expected to be enhanced (see Clarke, 1977). The infrared satellite image shown in Figure 1 clearly reveals a cold thermal intrusion (lighter colored regions) extending westward from Cape Mendocino. However, an examination of the bottom topography off the central California coast (see Fig. 2) shows that the Mendocino escarpment centered at 40N and extending westward for nearly 3000 km is likely to be a more important feature than Cape Mendocino for controlling the circulation in this region.

1. Department of Oceanography, Naval Postgraduate School, Monterey, California, 93943, U.S.A.
2. Present address: Department of Mathematics, University of Exeter, North Park Road, Exeter, England, EX4 4QE.
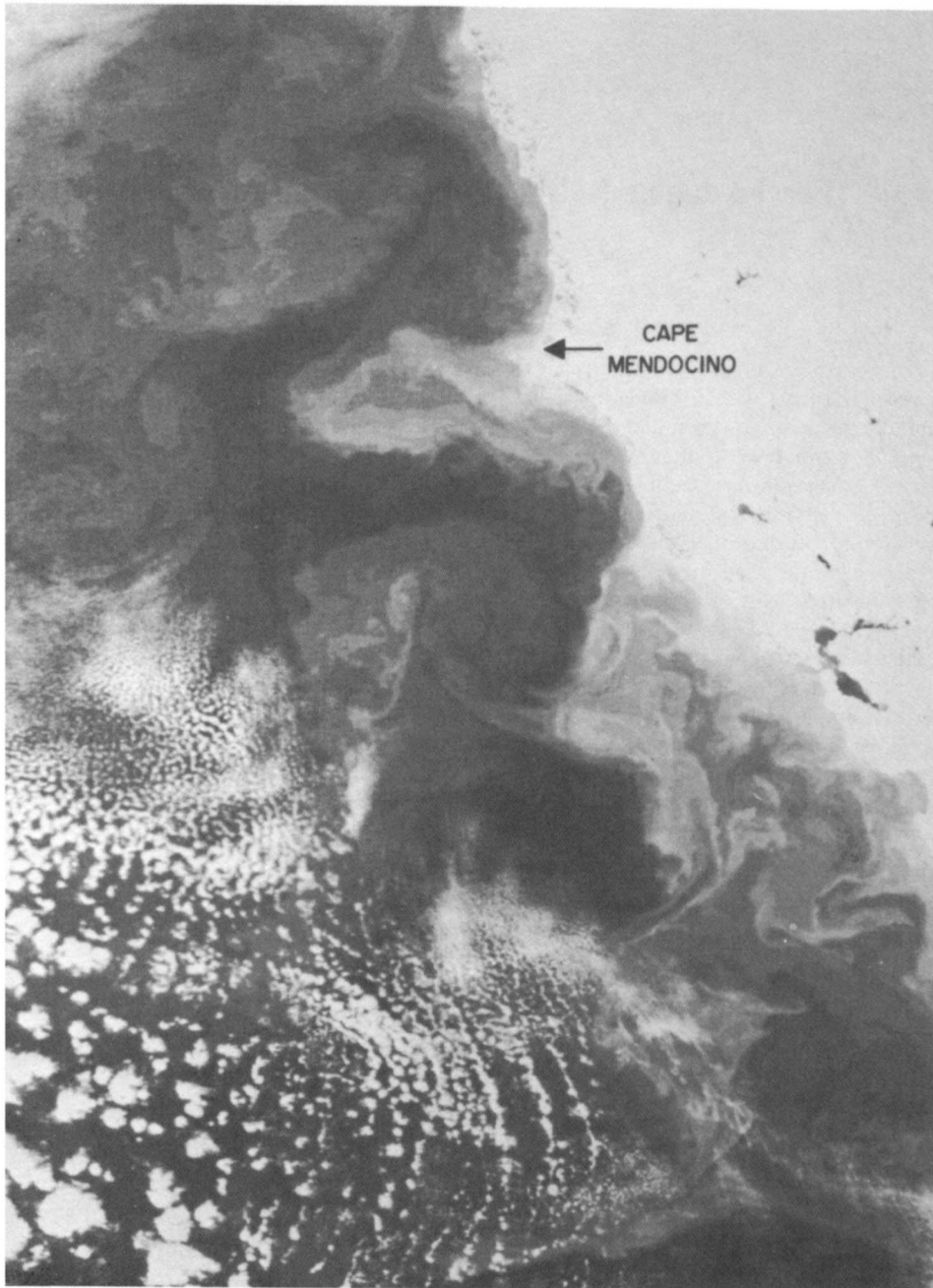
Figure 1. Satellite infrared image of the northern California coast on 16 October 1981. The presence of a cold water plume (lighter shaded region) originating from the enhanced upwelling zone around Cape Mendocino is clearly visible. The surface thermal pattern offshore from Cape Mendocino suggests that the presence of the underwater escarpment may be influencing the flow field in this region.
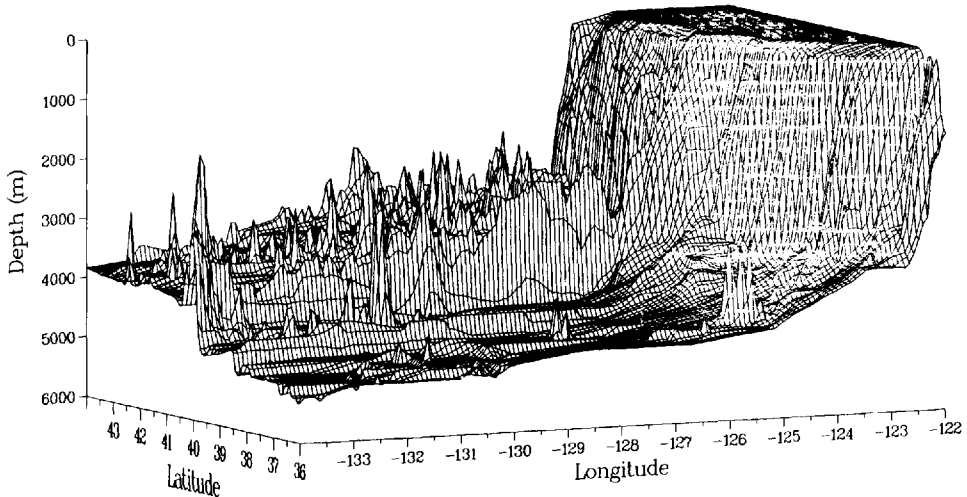
Mendocino Escarpment
Bathymetry

Figure 2. The bottom bathymetry off the northern California coast between 36N to 44N and 122W to 133W. The Mendocino escarpment is clearly visible, although numerous seamounts interrupt the steplike nature of the seascarp.

At the present time there are no data available for determining the depth of penetration of the cold water intrusions extending westward from Cape Mendocino. Breaker (1982, private communication) suggests that the cold water intrusions off Cape Mendocino are more persistent features than those occurring off other California headlands. This observation suggests that the flow field and thermal structure of the ocean off Cape Mendocino may be influenced by the presence of the undersea escarpment and the purpose of this paper is to elucidate upon such a coupling mechanism.

It is well known that a discontinuity in depth in a rotating ocean can act as a wave guide (see Longuet-Higgins, 1968a). In particular the subinertial double Kelvin wave exists over an abrupt single-step escarpment with phase propagating with shallow water on the right in the Northern Hemisphere. LeBlond and Mysak (1978) present an account of the propagation characteristics of the unforced double Kelvin wave in a homogeneous ocean. Mysak (1969) also considers the generation of a double Kelvin wave in a homogeneous ocean along an infinite escarpment by wind stress directed normal to the escarpment. In this study Mysak (1969) finds that when a nondivergent wind stress is suddenly applied to a quiescent ocean, the response consists of double

Kelvin waves which travel away from the forcing region with a maximum wavelength of about 10^4 km and an amplitude of about 1.5 cm. Mysak notes that the wavelength is unrealistically long and it is doubtful that the associated sea-surface elevation produced by these waves is measurable in the ocean. The purpose of this paper is to extend the model of Mysak (1969) to include the effects of stratification on the waves, by considering the response of a two-layer ocean to a nondivergent wind stress acting normal to a step escarpment of infinite extent. Rhines (1977) considers freely propagating double Kelvin waves over a step escarpment in a two-layer ocean. However there appears to be no treatment in the literature of the generation of double Kelvin waves in a two-layer ocean with a step-escarpment.

In Section 2 the normal mode equations in a wind forced two-layer ocean with a rigid upper surface are developed. The basic equations are reformulated in nondimensional form in Section 3. In Section 4 the dispersion relation for freely propagating double Kelvin waves is derived. A discussion of the free wave propagation characteristics as a function of the upper layer depth is presented. In Section 5 the partial differential equation governing the interfacial displacement is solved using transform techniques when a transient wind stress which has a step-function spatial dependence is suddenly applied to a quiescent ocean. Plots of the interfacial displacement along the escarpment as a function of time are presented in Section 6. The plots are obtained by numerically inverting the transform solution of Section 5. The dependence of the forced wave response over the escarpment on wind stress orientation is briefly discussed in Section 7. A spatially independent time-periodic wind stress is used in Section 7. Finally in Section 8 the shortcomings of the model and the direction for future research are discussed.

2. Basic equations

A right-handed cartesian coordinate system is chosen with the step escarpment lying vertically beneath the x-axis (see Fig. 3). In the case of Mendocino escarpment, shallow water lies to the north of the depth discontinuity and corresponds to the region $y < 0$ in Figure 3. The forced linearized two-layer long wave equations for a constant depth upper layer and variable depth lower layer $H_2(y)$ are given by

$$u_{1t} - fv_1 = -g\eta_{1x} + \frac{\tau^x}{\rho_1 H_1}, \tag{2.1}$$

$$v_{1t} + fu_1 = -g\eta_{1y} + \frac{\tau^y}{\rho_1 H_1}, \tag{2.2}$$

$$H_1 (u_{1x} + v_{1y}) - \eta_{2t} = 0, \tag{2.3}$$

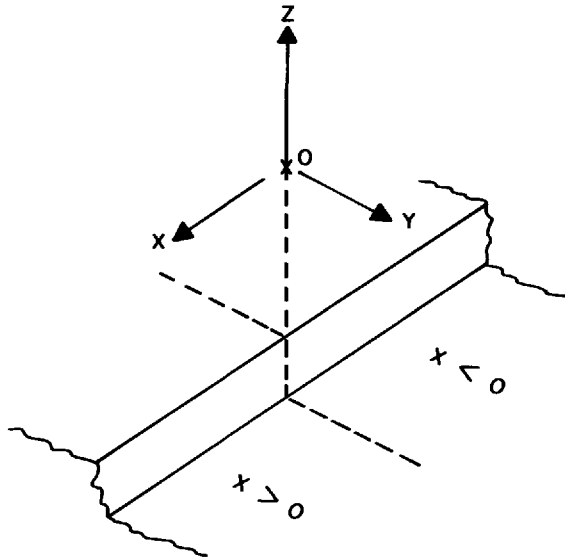$$u_{2t} - fv_2 = -g'\eta_{2x} - g\eta_{1x}, \tag{2.4}$$

Figure 3. Schematic representation of the orientation of the coordinate system with respect to the step escarpment of infinite horizontal extent.

$$v_{2t} + fu_2 = -g'\eta_{2y} - g\eta_{1y}, \tag{2.5}$$

$$H_2 u_{2x} + (H_2 v_2)_y + \eta_{2t} = 0, \tag{2.6}$$

where (u_1, v_1) (u_2, v_2) are the velocities in the upper and lower layers respectively; η_1, η_2 are the surface and interfacial displacements; τ^x, τ^y are the components of wind stress in the x and y directions; H_1, H_2 are the undisturbed depths of the upper and lower fluid layers which are taken as constant except for a step discontinuity in H_2 corresponding to the escarpment; g is the acceleration due to gravity and $g' = \mu g$ denotes reduced gravity where $\mu = (1 - \rho_1/\rho_2) \ll 1$. The system of equations (2.1) to (2.6) are discussed in some detail by Wright and Mysak (1977) and it will suffice to say that terms of relative magnitude μ have been neglected in (2.4) and (2.5). Also in (2.3) the rigid lid approximation has been made which eliminates all surface gravity waves and the external Kelvin wave from the system.

The step escarpment of infinite horizontal extent is described by

$$H_2 = \begin{cases} H_2^{(N)}, \text{ for } y < 0, \\ H_2^{(S)}, \text{ for } y > 0, \end{cases} \tag{2.7}$$

where $H_2^{(N)} < H_2^{(S)}$ and the superscripts (N) and (S) are used to distinguish variables to the north and to the south of the Mendocino escarpment respectively. Since the depth of the ocean in the regions $y < 0$ and $y > 0$ is constant, it is convenient to follow

the analysis technique adopted by Allen (1975) and Wright and Mysak (1977) in which the normal mode equations for a two-layer fluid on an f-plane are derived. For completeness a brief derivation of the normal mode equations is presented in this section. In the derivation the superscripts (N) and (S) are omitted on all dependent variables with the understanding that the analysis applies on either side of the escarpment.

When (2.3) and (2.6) are added, it is clear that a mass transport stream function ψ exists in which

$$\psi_x = H_1 v_1 + H_2 v_2, \tag{2.8}$$
$$\psi_y = -(H_1 u_1 + H_2 u_2).$$

For a constant depth two-layer ocean, system (2.1) to (2.6) can be reduced to two decoupled (normal mode) equations for ψ and η_2 (see Allen, 1975 and Wright and Mysak, 1977) in the following manner. When the system of Eqs. (2.1), (2.2), (2.4), (2.5) and (2.8) is solved for (u_1, v_1) and (u_2, v_2) in terms of ψ, η_2 and (τ^x, τ^y) the following expressions are obtained:

$$Lu_1 = \{-L(\psi_y) + g'H_2(\eta_{2xt} + f\eta_{2y}) + \frac{H_2}{\rho_1 H_1}(\tau_t^x + f\tau^y)\}/H, \tag{2.9a}$$

$$Lu_2 = \{-L(\psi_y) - g'H_1(\eta_{2xt} + f\eta_{2y}) - \frac{1}{\rho_1}(\tau_t^x + f\tau^y)\}/H, \tag{2.9b}$$

$$Lv_1 = \{L(\psi_x) + g'H_2(\eta_{2yt} - f\eta_{2x}) + \frac{H_2}{\rho_1 H_1}(\tau_t^y - f\tau^x)\}/H, \tag{2.9c}$$

$$Lv_2 = \{L(\psi_x) - g'H_1(\eta_{2yt} - f\eta_{2x}) - \frac{1}{\rho_1}(\tau_t^y - f\tau^x)\}/H, \tag{2.9d}$$

where $H = H_1 + H_2$ and $L \equiv \partial_{tt} + f^2$. Cross-differentiating (2.1) and (2.2) and using (2.3) yields the upper layer vorticity equation

$$(u_{1y} - v_{1x})_t - (f/H_1)\eta_{2t} = -\frac{1}{\rho_1 H_1}\mathbf{k} \cdot \text{curl } \tau. \tag{2.10}$$

A similar operation on (2.4), (2.5) and (2.6) yields the lower layer vorticity equation

$$(u_{2y} - v_{2x})_t + (f/H_2)\eta_{2t} = 0. \tag{2.11}$$

Adding (2.10) and (2.11) and employing (2.8) yields the first of the normal mode equations for ψ, namely

$$\nabla_H^2 \psi_t = \frac{1}{\rho_1}\mathbf{k} \cdot \text{curl } \tau \tag{2.12}$$

Eq. (2.12) describes the behavior of the barotropic part of the flow and describes a forced transient response. To derive the second normal mode equation for η_2, (2.10) is subtracted from (2.11) to give

$$(u_{2y} - v_{2x})_t - (u_{1y} - v_{1x})_t + f\left(\frac{1}{H_1} + \frac{1}{H_2}\right)\eta_{2t} = \frac{1}{\rho_1 H_1}\mathbf{k} \cdot \text{curl } \tau. \qquad (2.13)$$

The velocity components in the upper and lower layers appearing in (2.13) are eliminated in favor of ψ and η_2 by operating on (2.13) by L and employing (2.9). When L is approximated by f^2 (the internal double Kelvin waves have periods of several days) the final equation for η_2 is

$$\nabla_H^2 \eta_{2t} - \frac{1}{r_{i2}^2}\eta_{2t} = F, \qquad (2.14a)$$

where

$$r_{i2}^2 = \frac{g' H_1 H_2}{f^2 H}, \qquad (2.14b)$$

is the internal Rossby radius of deformation in a two-layer ocean and

$$F = -\frac{f}{\rho_1 g' H_1}\mathbf{k} \cdot \text{curl } \tau - \frac{1}{\rho_1 g' H_1}(\nabla \cdot \tau)_t. \qquad (2.14c)$$

The boundary conditions associated with (2.12) and (2.14) are that ψ and η_2 must remain bounded as $|y| \to \infty$. At the escarpment $y = 0$ the sea surface and interfacial displacements η_1 and η_2 must be continuous:

$$[\eta_1] = 0 = [\eta_2] \quad \text{at} \quad y = 0. \qquad (2.15)$$

The continuity condition on η_1 must be expressed in terms of ψ and η_2. Clearly η_{1x} must also be continuous at $y = 0$, which from (2.1) implies that

$$[u_{1t} - fv_1] = 0 \quad \text{at} \quad y = 0. \qquad (2.16)$$

The matching condition (2.16) can straightforwardly be rewritten in terms of ψ and η_2 using (2.9) and approximating L by f^2 to give

$$\left[-\frac{\psi_{yt}}{H} - f\frac{\psi_x}{H} + \frac{g' H_2}{H}\eta_{2x} + \frac{H_2}{\rho_1 H_1 H}\tau^x\right] = 0 \quad \text{at} \quad y = 0. \qquad (2.17)$$

At the escarpment the condition of continuous normal mass transport in each layer must also be imposed, which requires

$$[H_1 v_1] = 0 = [H_2 v_2] \quad \text{at} \quad y = 0. \qquad (2.18)$$

Adding together the transport normal to the escarpment in each layer gives, with the aid of (2.8)

$$[\psi_x] = 0 \quad \text{at} \quad y = 0. \tag{2.19}$$

To obtain the fourth matching condition at $y = 0$ the transport in the upper layer only is considered. Using (2.9c), the first of the matching conditions in (2.18) can be expressed as

$$\left[\frac{\psi_x}{H} + \frac{g'H_2}{f^2H}(\eta_{2yt} - f\eta_{2x}) + \frac{H_2}{\rho_1 H_1 H f^2}\tau_t^y - \frac{H_2}{\rho_1 H_1 H f}\tau^x\right] = 0 \quad \text{at} \quad y = 0. \tag{2.20}$$

3. Nondimensional equations

It is convenient to recast the governing equations in Section 2 into a nondimensional form by defining the dimensionless variables (denoted by an asterisk)

$$\left.\begin{array}{ll} (x, y) = L(x^*, y^*), & t = \sigma_0^{-1}t^*, \quad \tau = \tau_0\tau^* \\ \eta_2 = \eta_0\eta_2^*, & \psi = \psi_0\psi^* \end{array}\right\} \tag{3.1}$$

where $\eta_0 = \tau_0 L/(\rho_1 g'H_1)$, $\psi_0 = \tau_0 L/(\rho_1\sigma_0)$ and L, σ_0^{-1} and τ_0 are the length, time and stress magnitude scales which appear in the wind stress forcing. In rewriting the equations in Section 2 in dimensionless form it is convenient to introduce the nondimensional parameters

$$\Delta_N = \frac{H_1}{H_2^{(N)}}, \Delta_S = \frac{H_1}{H_2^{(S)}}, \tag{3.2a}$$

$$\gamma = \left(\frac{1 + \Delta_N}{1 + \Delta_S}\right) > 1, \tag{3.2b}$$

$$\delta = \sigma_0/f < 1. \tag{3.2c}$$

Furthermore, the governing dimensionless equations on either side of the escarpment will be stated separately, without the asterisks. When (3.1) is used to nondimensionalize (2.12) it is found that

$$\nabla_H^2\psi_t^{(N)} = \mathbf{k} \cdot \text{curl } \tau = \nabla_H^2\psi_t^{(S)}. \tag{3.3}$$

The dimensionless form of (2.14) is

$$\nabla_H^2\eta_{2t}^{(N)} - \epsilon\gamma\eta_{2t}^{(N)} = -\frac{1}{\delta}F, \tag{3.4a}$$

$$\nabla_H^2\eta_{2t}^{(S)} - \epsilon\eta_{2t}^{(S)} = -\frac{1}{\delta}F. \tag{3.4b}$$

where $\epsilon = [L/r_{i2}^{(S)}]^2$, $[r_{i2}^{(S)}]^2 = g'H_1H_2^{(S)}/(H^{(S)}f^2)$ and

$$F = \mathbf{k} \cdot \text{curl } \tau + \delta(\nabla \cdot \tau)_t. \tag{3.4c}$$

The second of the jump conditions (2.15) and jump condition (2.19) remain the same in dimensionless form, namely

$$\eta_2^{(N)} = \eta_2^{(S)} \quad \text{at} \quad y = 0, \tag{3.5a}$$

$$\psi_x^{(N)} = \psi_x^{(S)} \quad \text{at} \quad y = 0. \tag{3.5b}$$

However, when (2.17) is recast into dimensionless form the jump condition becomes

$$r_S\psi_{yt}^{(N)} - r_N\psi_{yt}^{(S)} = -\frac{1}{\delta}(\psi_x + \delta\eta_{2x}) - \tau^x \quad \text{at} \quad y = 0 \tag{3.6a}$$

where

$$r_S = \frac{H^{(S)}}{(H_2^{(S)} - H_2^{(N)})}, \, r_N = \frac{H^{(N)}}{(H_2^{(S)} - H_2^{(N)})}. \tag{3.6b}$$

Clearly the dimensionless parameters r_S and r_N satisfy

$$r_S - r_N = 1. \tag{3.6c}$$

On the right-hand side of (3.6a) the superscripts have been omitted because ψ_x and η_{2x} are both continuous across $y = 0$. Finally the dimensionless form of jump condition (2.20) is

$$\frac{r_N}{\Delta_S}\eta_{2yt}^{(S)} - \frac{r_S}{\Delta_N}\eta_{2yt}^{(N)} = \frac{1}{\delta^2}(\psi_x + \delta\eta_{2x}) - \tau_t^y + \frac{1}{\delta}\tau^x \quad \text{at} \quad y = 0. \tag{3.7a}$$

where the continuity of ψ_x, η_{2x} and τ_t^y has been exploited to allow the superscripts to be omitted on the right-hand side of (3.7a). It is useful to note that

$$\frac{r_N}{\Delta_S} - \frac{r_S}{\Delta_N} = 1, \tag{3.7b}$$

and

$$\frac{r_S}{\Delta_N} = \frac{1}{(\gamma - 1)}. \tag{3.7c}$$

The subsequent analysis is simplified by working with an alternative form of the jump condition (3.7a). If (3.6a) is multiplied by δ^{-1} and added to (3.7a) and the result then integrated once with respect to time, making use of (3.7b) and (3.7c), the following jump condition is obtained:

$$\frac{(\gamma - 1)}{\delta}[r_S\psi_y^{(N)} - r_N\psi_y^{(S)}] + \gamma\eta_{2y}^{(S)} - \eta_{2y}^{(N)}$$

$$= (\gamma - 1)(\tau^y|_{t-0} - \tau^y) \quad \text{at} \quad y = 0. \tag{3.8}$$

In deriving (3.8) it is further assumed that the ocean is at rest for $t \leq 0$.

To determine the flow field associated with forced double Kelvin waves, the nondimensional form of (2.9) is derived. The horizontal velocity components in both layers are nondimensionalized by $\tau_0/(\rho_1\sigma_0 H_1)$, which then allows the dimensionless form of (2.9) to be written as

$$u_1^{(N,S)} = -\frac{H_1}{H^{(N,S)}}\,\psi_y^{(N,S)} + \delta\,\frac{H_2^{(N,S)}}{H^{(N,S)}}\,\{\delta\eta_{2xt}^{(N,S)} + \eta_{2y}^{(N,S)} + \delta\tau_t^x + \tau^y\} \qquad (3.9a)$$

$$v_1^{(N,S)} = \frac{H_1}{H^{(N,S)}}\,\psi_x^{(N,S)} + \delta\,\frac{H_2^{(N,S)}}{H^{(N,S)}}\,\{\delta\eta_{2yt}^{(N,S)} - \eta_{2x}^{(N,S)} + \delta\tau_t^y - \tau^x\} \qquad (3.9b)$$

$$u_2^{(N,S)} = -\frac{H_1}{H^{(N,S)}}\,\{\psi_y^{(N,S)} + \delta^2\eta_{2xt}^{(N,S)} + \delta\eta_{2y}^{(N,S)} + \delta^2\tau_t^x + \delta\tau^y\} \qquad (3.9c)$$

$$v_2^{(N,S)} = \frac{H_1}{H^{(N,S)}}\,\{\psi_x^{(N,S)} - \delta^2\eta_{2yt}^{(N,S)} + \delta\eta_{2x}^{(N,S)} - \delta^2\tau^y + \tau^x\} \qquad (3.9d)$$

To summarize, the final nondimensional problem to be solved is given by Eqs. (3.3) to (3.6) and (3.8) when a wind stress is suddenly applied at $t = 0$, thereby making the problem an initial value type.

4. The free-wave properties

As a precursor to understanding the response of atmospherically forced internal double Kelvin waves, a discussion of the free-waves properties will be presented in this section.

The dispersion relation for double Kelvin waves in a two-layer ocean over a step discontinuity can be derived from the unforced version of (2.1) to (2.6), following the approach of Wright and Mysak (1977). Appendix A presents a brief outline of the derivation of the free wave dispersion relation. In dimensional form the dispersion relation is given by

$$\frac{\omega}{f} = \left(\frac{H_2^{(S)} - H_2^{(N)}}{H^{(S)} + H^{(N)}}\right)\left\{1 + \frac{kH_1(H^{(S)} + H^{(N)})}{[\lambda^{(N)}H_2^{(N)}H^{(S)} + \lambda^{(S)}H_2^{(S)}H^{(N)}]}\right\} \qquad (4.1a)$$

where

$$\lambda^{(N)} = (k^2 + 1/r_{i2}^{(N)2})^{1/2} \qquad (4.1b)$$

$$\lambda^{(S)} = (k^2 + 1/r_{i2}^{(S)2})^{1/2} \qquad (4.1c)$$

and ω, k are the angular frequency and along-escarpment wavenumber respectively.

It is convenient to recast (4.1) into dimensionless form by introducing a dimensionless wavenumber $\kappa = r_{12}^{(S)}k$ and frequency $\sigma = \omega/f$, in which case

$$\sigma = \frac{1}{R}\left\{1 + \frac{(\gamma - 1)\kappa R}{(\Gamma_2 + \gamma\Gamma_1)}\right\} \tag{4.2a}$$

where

$$\Gamma_1 = (\kappa^2 + 1)^{1/2}, \tag{4.2b}$$

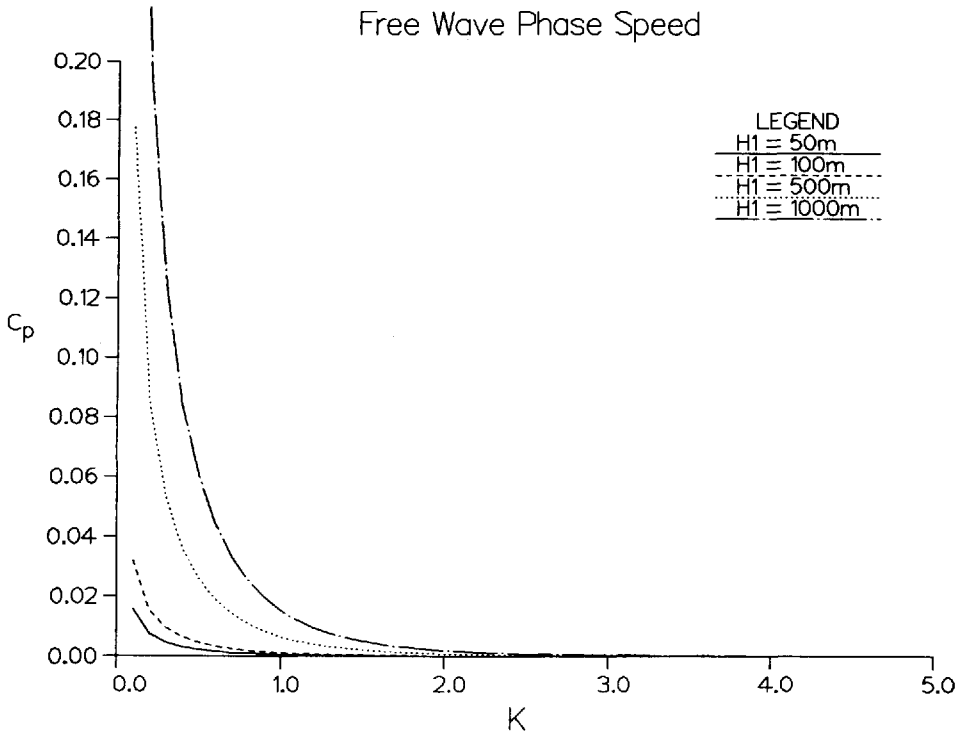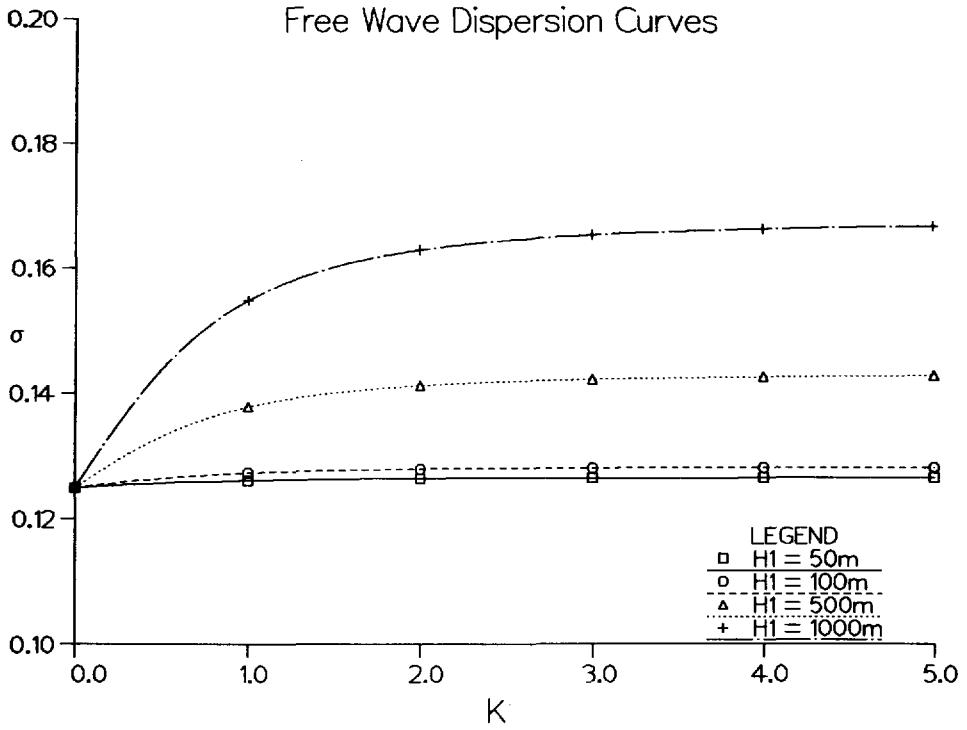$$\Gamma_2 = (\kappa^2 + \gamma)^{1/2}, \tag{4.2c}$$

$$R = r_s + r_N, \tag{4.2d}$$

and r_S, r_N and γ are defined in Section 3. The dimensionless phase speed $c = \sigma/\kappa$ and group speed $c_g = d\sigma/d\kappa$ are easily obtained from (4.2). Dispersion relation (4.2) is derived by Rhines (1977).

In Figure 4a, a plot of the dispersion relation (4.2a) with upper depth H_1 as a variable parameter, is presented. The values $H^{(N)} = 3500$ m and $H^{(S)} = 4500$ m are used and are representative for the Mendocino escarpment. Also displayed in Figure 4 are plots of the dimensionless phase speed c_p and group speed c_g, with H_1 as a parameter. As H_1 decreases (or the wavelength increases) the system exhibits barotropic double Kelvin wave behavior in which the frequency σ is almost independent of the wavenumber κ and the group speed c_g vanishes almost everywhere (see Fig. 4c). The vanishing of c_g in the homogeneous limit (or equivalently, the long wavelength regime) is a consequence of the surface rigid-lid approximation.

For intermediate values of the stratification (or the wavelength), the group speed is significantly nonzero and σ varies with wavelength. As the wavelength decreases ($\kappa \to \infty$) the waves become increasingly confined to the lower layer and the interfacial displacement acts as a rigid-lid. These bottom-intensified waves are noted by Rhines (1977). It can be seen from (4.2a) that

$$\sigma \to \frac{1}{R} + \frac{\gamma - 1}{\gamma + 1} \quad \text{as} \quad \kappa \to \infty.$$

Figure 5a displays the dispersion relation (4.2a) when $H_1 = 500$ m, $H^{(N)} = 3500$ m, $H^{(S)} = 4500$ m, $g' = 0.5 \times 10^{-2}$ m s^{-2} and $f = 0.937 \times 10^{-4}$ s^{-1} (corresponding to a latitude of 40N). These parameter values are representative of the Mendocino escarpment and are discussed further in Section 6. Also displayed on Figure 5a are the dimensional wavelength and wave period. Figures 5b and c show the corresponding dimensional phase and group speed as a function of dimensional wavelength respectively.

Free Wave Dispersion Curves

LEGEND
□ H1 = 50m
○ H1 = 100m
△ H1 = 500m
+ H1 = 1000m

Free Wave Phase Speed

LEGEND
H1 = 50m
H1 = 100m
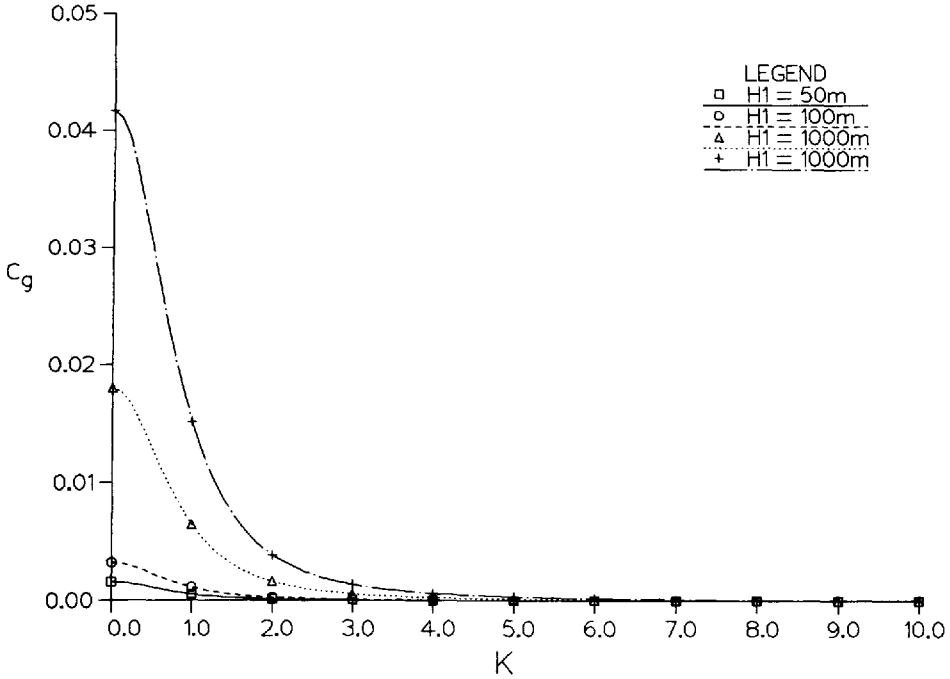H1 = 500m
H1 = 1000m

Free Wave Group Velocity

Figure 4. (a) Free wave dispersion curves with the upper layer depth H_1 as a parameter; (b) Free wave phase speed c_p plotted against dimensionless wavenumber κ with the upper layer depth H_1 as a parameter; (c) Free wave group speed c_g plotted against dimensionless wavenumber κ with the upper layer depth H_1 as a parameter.

5. Response to a transient wind stress

The internal double Kelvin wave response generated by the sudden intensification and gradual decay of a large anticyclonic weather system centered over the escarpment will be calculated in this section. Following Mysak (1969), a wind stress of this form can be modelled by

$$\tau^x = 0, \quad \tau^y = \tau_0 H(t)H(x)e^{-\sigma_0 t}, \tag{5.1}$$

where $\sigma_0, \tau_0 > 0$ and H is the Heaviside step function. When nondimensionalizing, the time scale σ_0^{-1} and the stress scale τ_0 must clearly be used. However, Mysak (1969) points out that (5.1) has no specific length scale L. It is natural to choose $L = r_{l2}^{(S)}$ (the natural trapping scale for wave motions over a topographic feature in a two-layer ocean), in which case $\epsilon = 1$. In dimensionless form (4.1) becomes

$$\tau^x = 0, \quad \tau^y = H(t)H(x)e^{-t}, \tag{5.2}$$
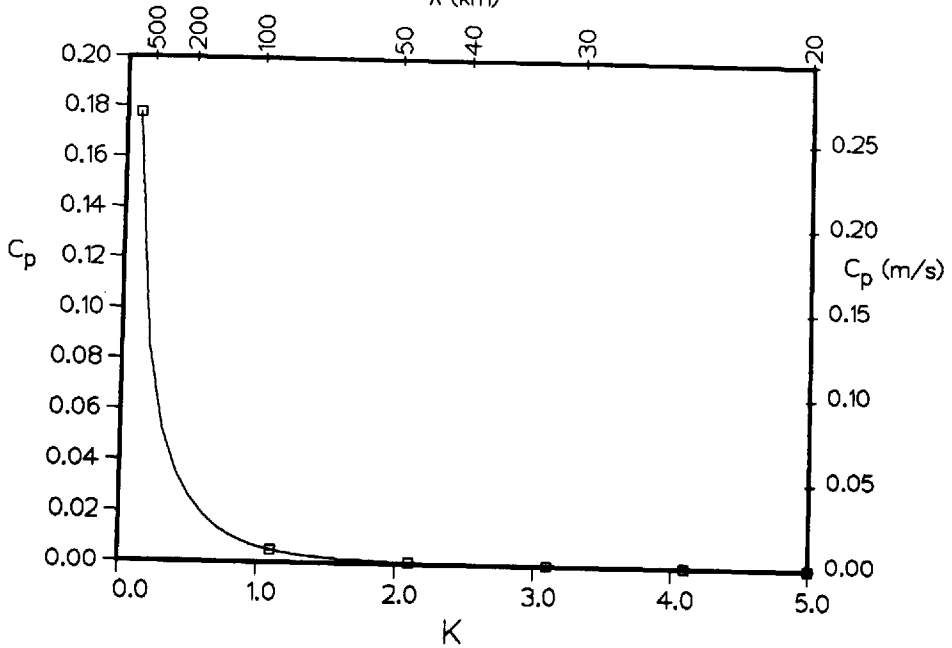
Free Wave Dispersion Curve
$H_1 = 500$ m
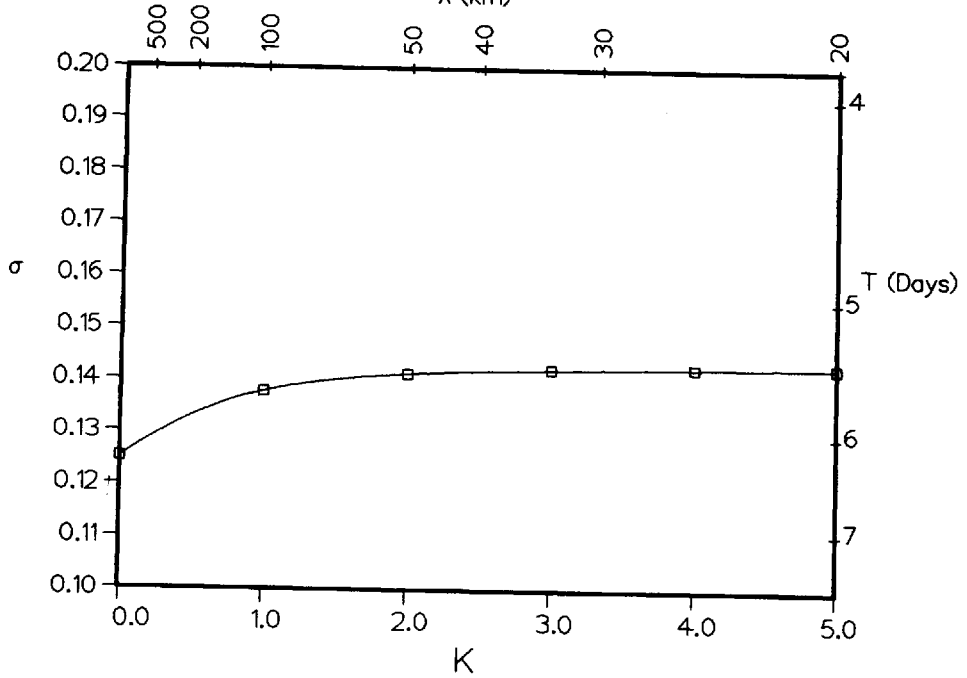
Free Wave Phase Speed
$H_1 = 500$ m

Free Wave Group Velocity
$H_1 = 500$ m
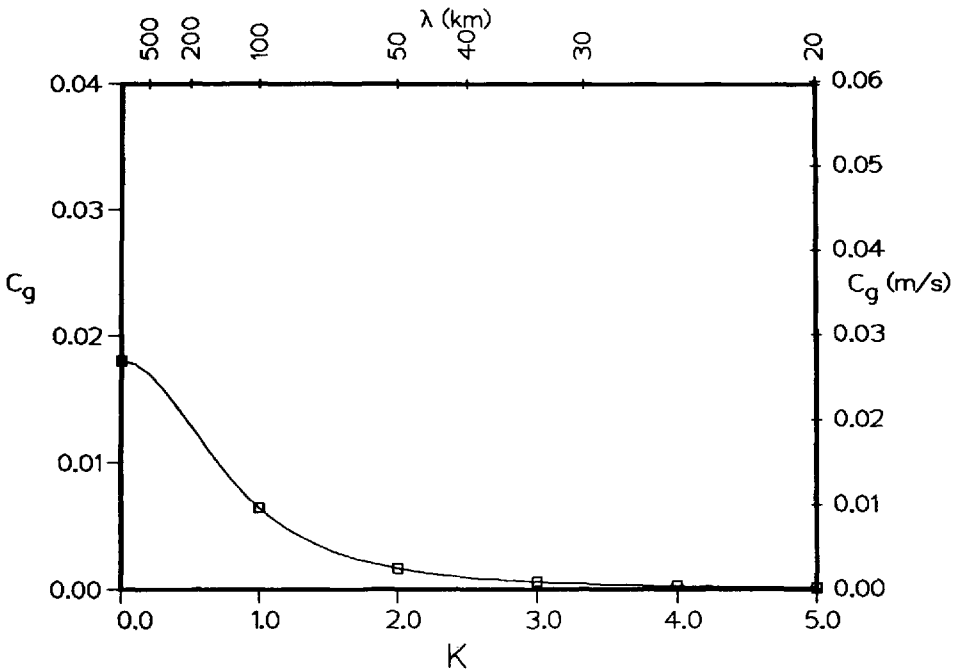

Figure 5. (a) Free wave dispersion curve with $H_1 = 500$ m; (b) Free wave phase speed c_p plotted as a function of dimensionless wavenumber with $H_1 = 500$ m; (c) Free wave group speed c_g plotted as a function of dimensionless wavenumber κ with $H_1 = 500$ m.

when the asterisks are omitted. The corresponding wind stress curl is given by

$$\mathbf{k} \cdot \mathrm{curl}\, \tau = H(t)\delta(x)e^{-t}, \tag{5.3}$$

however, the wind stress (5.2) is divergence-free.

To solve the problem stated in Section 3 a Laplace transform in time and a Fourier transform in x (along the escarpment) is employed. For any function $g(x, y, t)$ for which both these transforms exist, define

$$\tilde{g}(k, y, t) = \int_{-\infty}^{\infty} g(x, y, t)e^{-ikx}dx,$$

and

$$\bar{g}(k, y, s) = \int_{0}^{\infty} \tilde{g}(k, y, t)e^{-st}dt.$$

Assuming that η_2, ψ, η_{2x} and $\psi_x \to 0$ as $|x| \to \infty$ the transformed forms of (3.3) and

(3.4) become

$$\bar{\psi}_{yy} - k^2\bar{\psi} = \frac{1}{s(s + 1)}, \tag{5.4}$$

$$\bar{\eta}_{2yy}{}^{(S)} - K_1{}^2\bar{\eta}_2{}^{(S)} = \frac{-1}{s(s + 1)\delta}, \tag{5.5a}$$

$$\bar{\eta}_{2yy}{}^{(N)} - K_2{}^2\bar{\eta}_2{}^{(N)} = \frac{-1}{s(s + 1)\delta}, \tag{5.5b}$$

where

$$K_1{}^2 = k^2 + 1, K_2{}^2 = k^2 + \gamma \tag{5.5c}$$

and (5.4) is valid for both $\bar{\psi}^{(N)}$ and $\bar{\psi}^{(S)}$. The bounded solutions to (5.4) on either side of the escarpment which satisfy the transformed jump condition (3.5b) are given by

$$\bar{\psi}^{(N)} = \frac{-1}{s(s + 1)k^2} + Ae^{|k|y}, \quad y < 0, \tag{5.6a}$$

$$\bar{\psi}^{(S)} = \frac{-1}{s(s + 1)k^2} + Ae^{-|k|y}, \quad y > 0, \tag{5.6b}$$

where A is an arbitrary constant of integration, to be determined. Similarly, the bounded solutions to (5.5) are given by

$$\bar{\eta}_2{}^{(N)} = \frac{1}{s(s + 1)\delta K_2{}^2} + B_2 e^{K_2 y}, \quad y < 0, \tag{5.7a}$$

$$\bar{\eta}_2{}^{(S)} = \frac{1}{s(s + 1)\delta K_1{}^2} + B_1 e^{-K_1 y}, \quad y > 0, \tag{5.7b}$$

where B_1 and B_2 are constants to be determined. When the transformed form of jump condition (3.5a) is applied to (5.7) it is found that

$$B_2 - B_1 = \frac{(\gamma - 1)}{s(s + 1)\delta K_1{}^2 K_2{}^2}. \tag{5.8}$$

Furthermore, the transformed form of (3.6a) becomes

$$r_S\bar{\psi}_y{}^{(N)} - r_N\bar{\psi}_y{}^{(S)} = -\frac{ik}{s\delta}(\bar{\psi} + \delta\bar{\eta}_2), \quad \text{at} \quad y = 0. \tag{5.9}$$

On employing (5.6) and (5.7) in (5.9) a second equation relating A, B_1 and B_2 is found, namely

$$A(R + \frac{i}{s\delta}) + \frac{i}{s}B_1 = \frac{i}{s^2(s + 1)\delta k^2 K_1{}^2}, \tag{5.10}$$

where R is defined in (4.2d). The third equation relating A, B_1 and B_2 is found by first transforming (3.8) to obtain

$$\frac{(\gamma - 1)}{\delta} (r_S \bar{\psi}_y^{(N)} - r_N \bar{\psi}_y^{(S)}) + \gamma \bar{\eta}_{2y}^{(S)} - \bar{\eta}_{2y}^{(N)} = \frac{(\gamma - 1)}{s(s + 1)} G(k), \qquad (5.11)$$

where $G(k) = (ik)^{-1} + \pi\delta(k)$ and represents the complex Fourier transform of the Heaviside step function (see Lighthill, 1958, Ch. 3) that appears in τ^y. On substituting (5.6) and (5.7) into (5.11) it is found that

$$\frac{(\gamma - 1)kR}{\delta} A - \gamma K_1 B_1 - K_2 B_2 = \frac{(\gamma - 1)}{s(s + 1)} G. \qquad (5.12)$$

The system of Eqs. (5.8), (5.10) and (5.12) allows A, B_1 and B_2 to be determined.

Since the focus of this paper is to examine the behavior of the forced double internal Kelvin wave, attention will be focused on the solution for η_2. In particular the amplitude of the Kelvin wave response will be largest in the neighborhood of the escarpment itself and therefore the details of the solution $\eta_2(x, 0, t)$ will be calculated. Clearly

$$\bar{\eta}_2(k, 0, s) = \frac{1}{s(s + 1)\delta K_1^2} + B_1, \qquad (5.13)$$

where the superscript has been omitted in (5.13) because of the continuity of $\bar{\eta}_2$ across the escarpment. When (5.8), (5.10) and (5.12) are solved for B_1 it is found that

$$B_1 = \text{TERM 1/TERM 2} \qquad (5.14)$$

where

$$\text{TERM 1} \equiv (\gamma - 1)$$
$$\cdot \left[\frac{iR}{s(s + 1)\delta k K_1^2} - \frac{R}{(s + 1)K_1^2 K_2} - \frac{i}{s(s + 1)\delta K_1^2 K_2} - \frac{\delta RG}{(s + 1)} - \frac{iG}{s(s + 1)} \right]$$

and

$$\text{TERM 2} \equiv i(\gamma - 1)kR + (i + s\delta R)(K_2 + \gamma K_1).$$

In the absence of the escarpment, $\gamma = 1$, and $B_1 = 0$ which implies that η_2 will not exhibit wavelike behavior along the escarpment.

The Laplace transform inversion of (5.13) is formally obtained by evaluating the s-plane integral

$$\bar{\eta}_2(k, 0, t) = \frac{1}{2\pi i} \int_{u-i\infty}^{u+i\infty} \bar{\eta}_2(k, 0, s) e^{st} ds. \qquad (5.15)$$

An examination of (5.14) shows that in the s-plane the only singularities of the

integrand in (5.15) are the simple poles at $s = -1, 0$ and $-i\omega(k)$ where

$$\omega(k) = \frac{1}{\delta R}\left[1 + \frac{(\gamma - 1)kR}{(K_2 + \gamma K_1)}\right], \qquad (5.16)$$

and therefore the evaluation of (5.15) is straightforward. For $t > 0$ it is found that (5.15) is comprised of the sum of a steady state contribution $\tilde{\eta}_2^S$, a transient component $\tilde{\eta}_2^T$, and wavelike terms $\tilde{\eta}_2^W$, where

$$\tilde{\eta}_2^S = \frac{1}{\delta K_1^2} + \frac{(\gamma - 1)}{\delta K_1^2 D_2}\left(\frac{R}{k} - \frac{1}{K_2}\right) - \frac{(\gamma - 1)G(k)}{D_2} \qquad (5.17a)$$

$$\tilde{\eta}_2^T = -e^{-t}\left\{\frac{1}{\delta K_1^2}\left[1 + \frac{(\gamma - 1)}{D_1}\left\{\frac{iR}{k} + \frac{\delta R}{K_2} - \frac{i}{K_2}\right\}\right] + \frac{(\gamma - 1)G(k)}{D_1}(\delta R - i)\right\}, \quad (5.17b)$$

$$\tilde{\eta}_2^W = -(\gamma - 1)e^{-i\omega(k)t}\left\{\frac{1}{\delta K_1^2 D_3}\left(\frac{R}{k} - \frac{1}{K_2}\right) + \frac{R}{K_1^2 K_2 D_4} + G(k)\left(\frac{R}{D_4} - \frac{1}{D_3}\right)\right\}, \quad (5.17c)$$

and

$$D_1 = (i - \delta R)(K_2 + \gamma K_1) + i(\gamma - 1)kR,$$
$$D_2 = K_2 + \gamma K_1 + (\gamma - 1)kR,$$
$$D_3 = \omega(1 - i\omega)\delta R(K_2 + \gamma K_1),$$
$$D_4 = (1 - i\omega)\delta R(K_2 + \gamma K_1).$$

Before proceeding with the inversion of (5.17) it is worth noting what happens when there is no escarpment. In the absence of an escarpment, $\gamma = 1$, and all the wavelike terms (5.17c) vanish. Furthermore the coefficients A, B_1 and B_2 are zero and therefore (5.6) and (5.7) reduce to

$$\bar{\eta}_2(k, y, s) = \frac{1}{s(s + 1)\delta K_1^2}, \qquad (5.18a)$$

$$\bar{\psi}(k, y, s) = \frac{-1}{s(s + 1)K^2}. \qquad (5.18b)$$

The inversion of (5.18) is straightforward and yields

$$\eta_2(x, y, t) = \frac{1}{2\delta}(1 - e^{-t})e^{-|x|}, \quad t \geq 0 \qquad (5.19a)$$

$$\psi(x, y, t) = -\frac{1}{2}x\,sgn(x)(1 - e^{-t}), \quad t \geq 0. \qquad (5.19b)$$

It can be seen from (5.19) that the y-dependence of the problem vanishes and that

when the forcing is essentially zero ($t \rightarrow \infty$) a steady-state response is set up in which

$$\left.\begin{array}{l} \eta_2(x, t) = \dfrac{1}{2\delta}\, e^{-|x|}, \\[4mm] H_1 v_1 + H_2 v_2 = \psi_x = -\dfrac{1}{2}\, sgn\,(x), \end{array}\right\} \quad -\infty < y < \infty \qquad (5.20)$$

Solution (5.20) describes a tentlike elevation for η_2, the axis of which passes through the origin of the delta function curl and is parallel to the wind stress direction. The total transport parallel to the y-axis is clearly

$$H_1 v_1 + H_2 v_2 = \psi_x = -\frac{1}{2}\, sgn(x),$$

on employing (5.20). The final steady state flow is in geostrophic balance, and the work done by the transient wind stress goes into displacing the interface η_2.

The inversion of (5.17) cannot be performed analytically. To proceed using a numerical approach, the integral

$$\eta_2(x, 0, t) = \frac{1}{2\pi} \int_{-\infty}^{\infty} \tilde{\eta}_2(k, 0, t) e^{ikx} dx, \qquad (5.21)$$

must be evaluated. However when (5.17) is substituted into (5.21) certain resulting integrals contain integrands which have a factor k^{-1} and behave like Cauchy Principal Value (CPV) integrals. To avoid the complications associated with numerically evaluating CPV integrals it is useful to utilize the fact that

$$\int_{-\infty}^{\infty} \eta_{2x}(x, 0, t) e^{-ikx} dx = ik\tilde{\eta}_2(k, 0, t).$$

The solution given by (5.17) is multiplied by (ik) (thereby removing the k^{-1} factor in some terms on the right-hand side of (5.17)) which then gives the transform of $\partial \eta_2(x, 0, t)/x$. This expression can be inverted numerically to give $\partial \eta_2(x, 0, t)/\partial x$. Furthermore, for any fixed time t_0 the function $\partial \eta_2(x, 0, t_0)/\partial x$ can be numerically integrated with respect to x to yield $\eta_2(x, 0, t_0)$. The arbitrary constant of integration is determined by imposing the condition that $\eta_2 \rightarrow 0$ as $x \rightarrow \infty$. The accurate numerical evaluation of Fourier integrals is difficult and in Appendix B a brief discussion of the numerical technique used to evaluate $\partial \eta_2(x, 0, t)/\partial x$ is presented.

Finally it is worth noting that (5.16) is essentially the dispersion relation for free-propagating double Kelvin waves, which has been derived more generally in Section 4.

6. Results

From Section 5, it is clear that the solution for η_2 consists of the superposition of steady state, transient and wavelike terms corresponding to the contribution to the

total solution from the poles at $s = 0$, -1 and $-i\omega(k)$ respectively. The steady state and wavelike parts of the solution for η_2 will be displayed separately. Furthermore the contribution to the solution from the transient terms is small after the first unit of dimensionless time has elapsed from when the wind stress is applied and will not be displayed. Each of the three contributions to the total solution decay to zero independently as $x \rightarrow \infty$.

In all the model runs presented the total depth $(H_1 + H_2^{(N)})$ of the ocean on the poleward side of the escarpment is chosen to be 3500 m while on the equatorward side the total depth $(H_1 + H_2^{(S)})$ is 4500 m. This results in an average height for the Mendocino escarpment of 1000 m. Table 1 presents a summary of the parameter values chosen in five model runs. The parameter values assigned in Experiments 1 and 2 are likely to best model the wind-driven response over Mendocino escarpment. The values of $H_1 = 500$ m and $g' = 0.5 \times 10^{-2}$ m s^{-2} were found by Mysak (1977) to be suitable for the Northeast Pacific at a latitude of 49N. Throughout the parameter study the wind stress scaling factor $\tau^* = 3 \times 10^{-1}$ kg m^{-1} s^{-2}. Only the solution in the region $x > 0$ will be displayed, although there is a nonzero response in the region $x < 0$. However, for $x < 0$ the solution decays exponentially with increasing values of $-x$ (in a manner similar to that described by Mysak, 1969). The region $x > 0$ corresponds to the model ocean domain, where a nonzero wind stress acts normal to the escarpment.

Experiment 1. In this case a 500 m upper layer depth is chosen, which corresponds to the depth at which the pycnocline is most pronounced, and consequently will be the region where internal double Kelvin wave dynamics should be most important. In Figure 6 the steady parts of $\partial\eta_2/\partial x$ and η_2 are plotted as a function of distance along the escarpment from the wind stress curl origin. As expected the interface is upwelled by approximately 16 m at the origin of the delta function wind stress curl. At a distance of 95.4 m (6 units) along the escarpment, the steady state response is essentially zero. Within the first 32 km from the origin (2 units) the steady state contribution does in fact dominate the contribution from the wavelike terms in the solution for η_2 and $\partial\eta_2/\partial x$. This is clearly seen in Figures 7 and 8. In Figure 7 the function $\partial\eta_2/\partial x$ is plotted against distance along the escarpment at nine distinct times indicated in the figure. Plots of $\partial\eta_2/\partial x$ are presented because the wavelike behavior of the solution is particularly well exhibited by this quantity.

After the wind stress is first applied a large wave is generated in the neighborhood of the wind stress curl origin (See Fig. 7a), the phase of which propagates with shallow water on the right. At later times, Figure 7b, c show that smaller amplitude dispersive waves are successively generated at the origin and propagate in the wake of the primary wave. Mysak (1969) noted analogous behavior for the forced external double Kelvin wave. At each of the times displayed in Figure 7, the function $\partial\eta_2/\partial x$ is numerically integrated with respect to x to calculate the corresponding behavior of η_2 along the escarpment and the results are displayed in Figure 8. During the first 10

Table 1. Parameter values assigned in the five numerical experiments. In all the experiments the escarpment is located at 40N and the scaling factor used for the wind stress τ^* is given by $\tau^* = 3 \times 10^{-1}$ kg m^{-1} s^{-2}.

Parameter study experiment number	Upper layer depth H_1(m)	Reduced gravity g'(ms^{-2})	$\delta = \sigma_0 f^{-1}$	*e*-folding time scale of the wind stress σ_0^{-1} (days)	Internal Rossby radius $r_{i2}^{(S)}$ (km)	Scale factor of the interfacial displacement η_0(m)
1	500	$.5 \times 10^{-2}$	.05	2.4	15.9	1.91
2	500	$.5 \times 10^{-2}$	.10	1.2	15.9	1.91
3	500	2×10^{-2}	.05	2.4	31.8	0.95
4	100	$.5 \times 10^{-2}$	.05	2.4	7.1	4.27
5	100	2×10^{-2}	.05	2.4	14.2	2.13

units of time after the wind stress is applied the wavelike behavior of η_2 is dominated by the steady state contribution to η_2. However, as time evolves the primary wave propagates further along the escarpment into the region where the steady state response almost vanishes (see Fig. 7b). Figure 7c shows the later development of η_2 as a function of distance along the escarpment. In Figure 8c, the amplitude of the oscillation of η_2 is approximately 1.5 units for the primary wave at $t = 30$. In
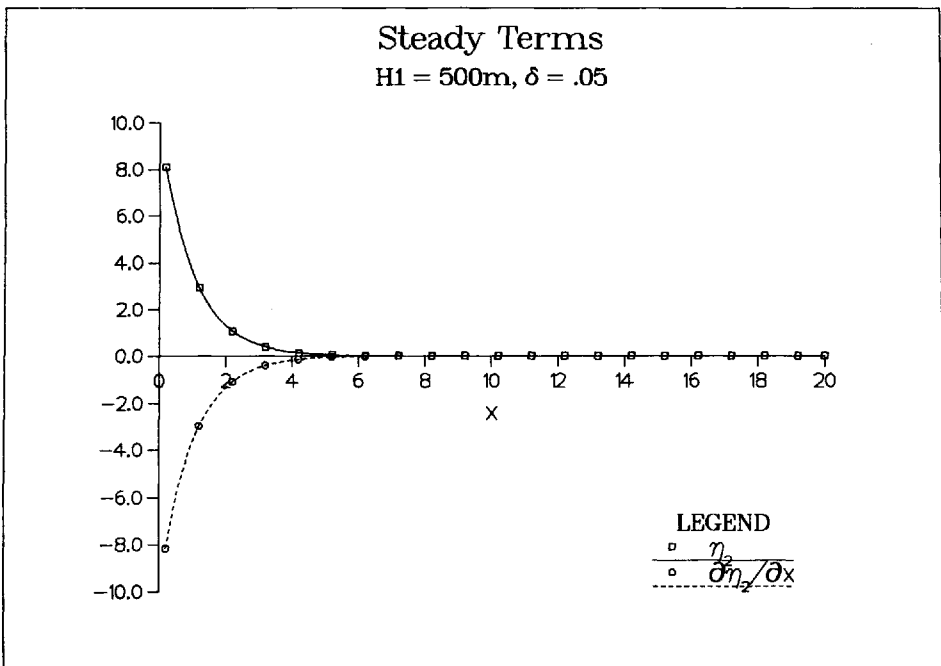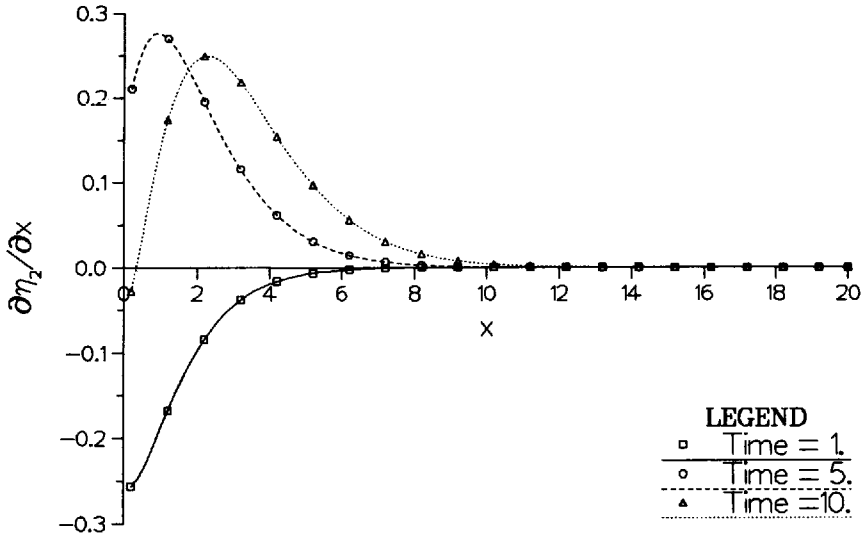

Figure 6. Plot of the steady state contribution to the total solution for $\partial\eta_2/\partial x$ and η_2 over the escarpment for $x \geq 0$. The parameter values chosen are given in Table 1 under Experiment 1.
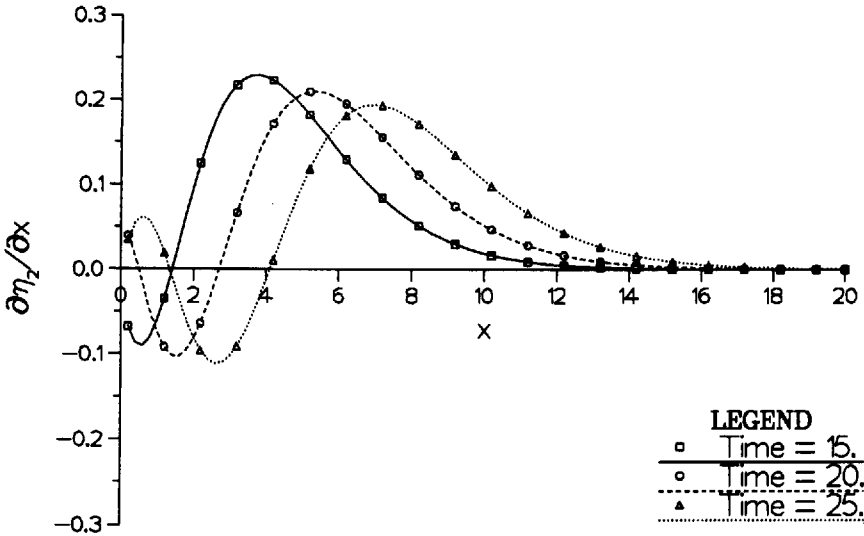
Wave–like Terms
H1 = 500m, δ = .05

LEGEND
□ Time = 1.
○ Time = 5.
▲ Time =10.

Wave–like Terms
H1 = 500m, δ = .05
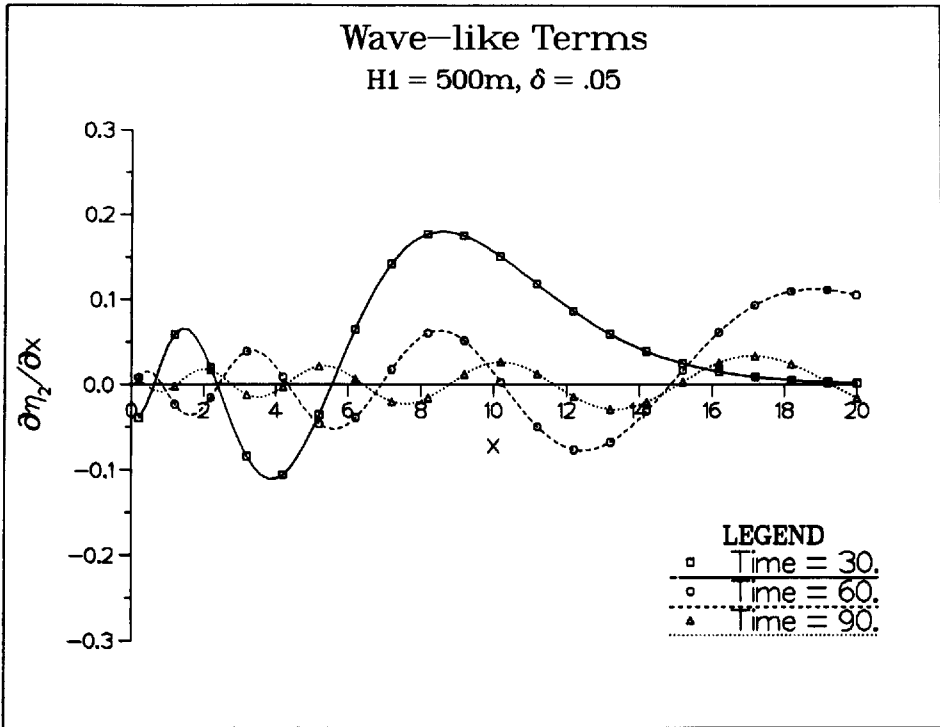
LEGEND
□ Time = 15.
○ Time = 20.
▲ Time = 25.

Figure 7. Plot of the wave contribution to the total solution for $\partial \eta_2 / \partial x$ over the escarpment for $x \geq 0$. The wavelike terms are plotted with dimensionless time t as a parameter: (a) $t = 1.0$, 5.0, 10.0; (b) $t = 15.0, 20.0, 25.0$; (c) $t = 30.0, 60.0, 90.0$. The parameter values chosen are the same as those in Figure 6.

dimensional units this means that 72 days after the sudden intensification and decay of the wind stress directed normal to the escarpment the amplitude of the primary wave generated is approximately 2.97 m at a distance of 80 km from the wind stress and origin. The total interfacial excursion will almost be 6 m at that time.

For large times it is found numerically that the wave response dies away. This perhaps is not surprising because the waves generated by the transient forcing are dispersive. The free wave dispersion curves calculated in Section 4 do not describe the large time response when the forcing has vanished. The asymptotic $(\kappa - \sigma)$ pair does not lie on the dispersion curve in Figure 5a implying that the waves must therefore decay. For values of $\kappa > 4$, Figure 5c shows that the group velocity of the free waves is essentially zero. If double Kelvin waves are impulsively excited and then at a later time the forcing is removed, a large time response can be achieved in which the waves will not die away. In this case the waves will have a dimensionless wavenumber satisfying the condition $\kappa > 4$.

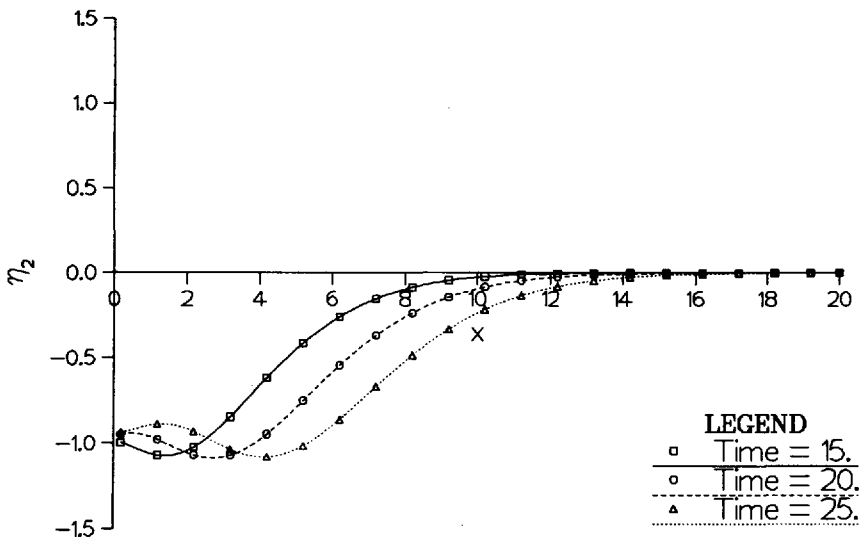It is difficult to assign a value for the wavelength associated with the forced primary

Wave−like Terms

H1 = 500m, δ = .05

LEGEND

□	Time = 1.
○	Time = 5.
△	Time = 10.

Wave−like Terms

H1 = 500m, δ = .05

LEGEND
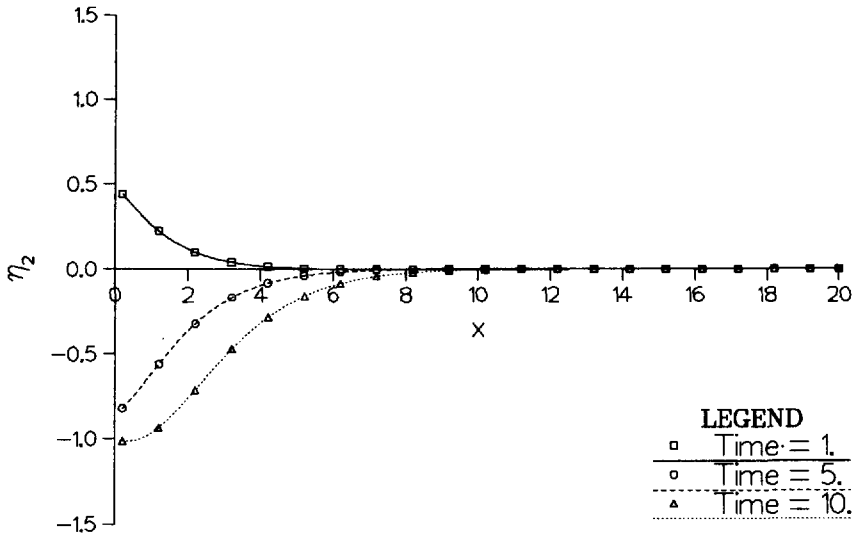
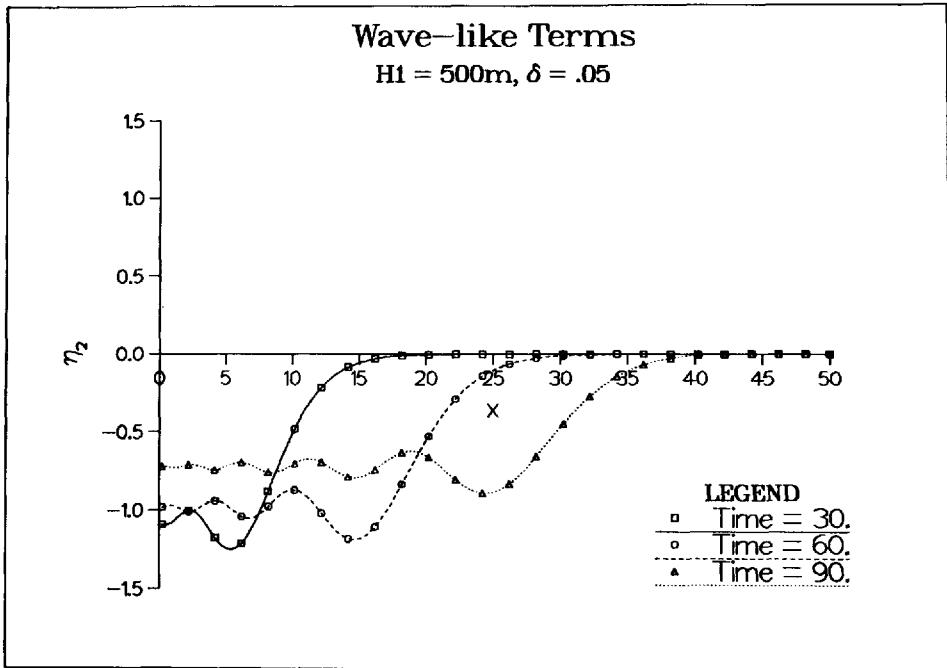|	
□	Time = 15.
○	Time = 20.
△	Time = 25.

Figure 8. As in Figure 7, except the wave contribution to the total solution for η_2 is plotted as a function of x over the escarpment with dimensionless time as a parameter.

wave in the solution for η_2 because of the complicated oscillatory behavior along the escarpment at any fixed time. However the distance along the escarpment from where η_2 is essentially zero to where $\partial\eta_2/\partial x$ first vanishes appears to be a suitable choice for the wavelength. In Figure 8c this distance is approximately 15 units which corresponds to 238.5 km. As expected the wavelength and phase speed of the forced internal double Kelvin waves are less than the corresponding quantities associated with the homogeneous wave solutions examined by Mysak (1969). The phase speed of the forced primary wave associated with η_2 varies with location along the escarpment. An average value for the phase speed calculated from Figure 8c is 2 km day^{-1}.

To facilitate understanding the temporal behavior of the waves, a plot of $\partial\eta_2/\partial x$ as a function of time at 32 km and 159 km from the origin is displayed in Figure 9. The plots displayed in Figure 9 are also representative of the temporal behavior of η_2 and show that both amplitude and phase modulation occurs. It is easy to explain why amplitude modulation occurs by examining typical integrals in the Fourier inversion of (5.17). Consider

$$I = \int_{-\infty}^{\infty} F(k) \cos [kx - \omega(k)t] \, dk$$

where $F(k) \rightarrow 0$ as $|k| \rightarrow \infty$ and $\omega(k)$ is given by (5.16). After some algebra it is found
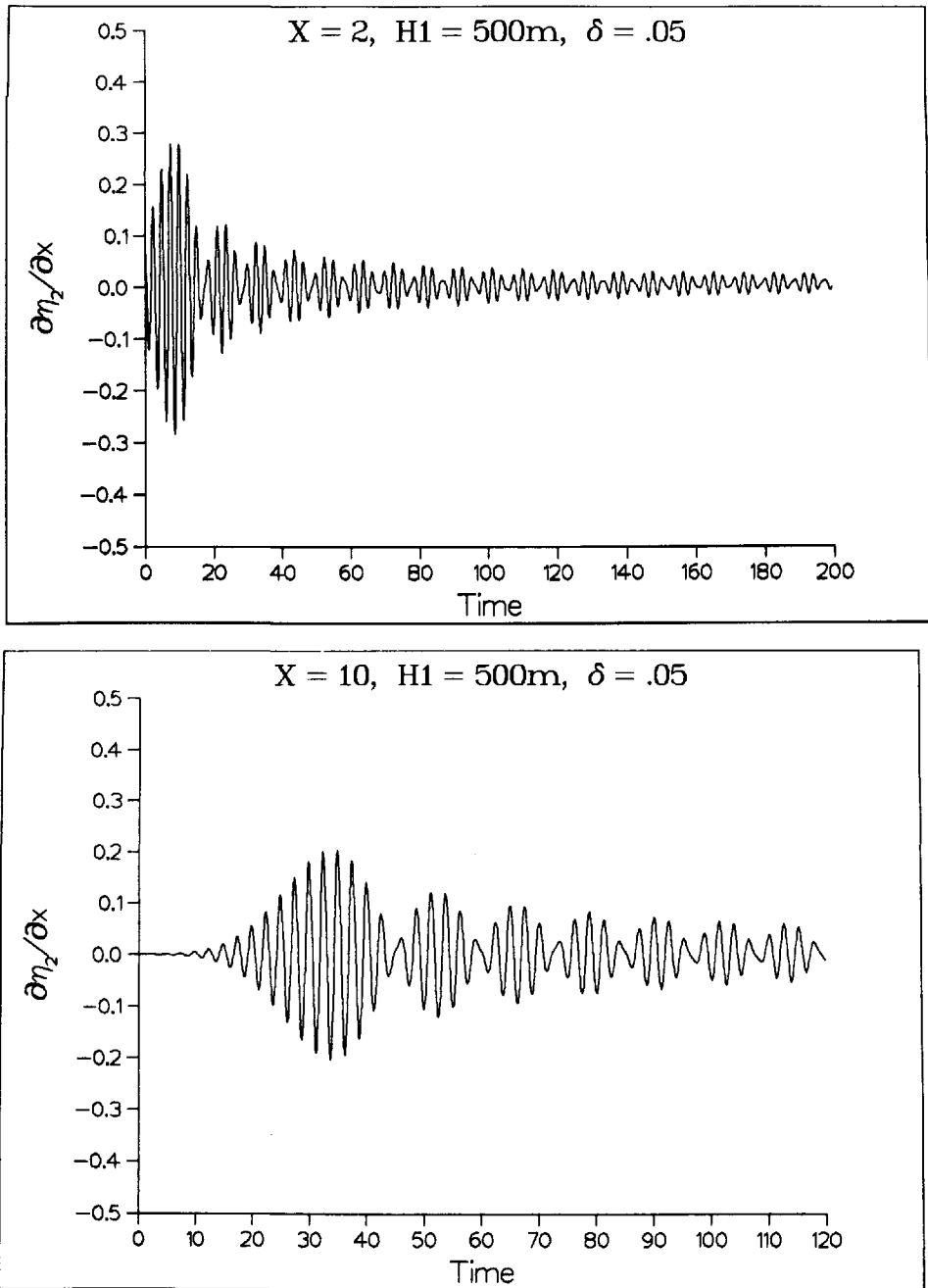
Figure 9. Plot of the wave contribution to $\partial \eta_2 / \partial x$ as a function of dimensionless time, at two locations over the escarpment. In case (a) $x = 2$ and (b) $x = 10$. The parameter values chosen are the same as those in Figure 4.

that

$$I = \cos\left(\frac{t}{\delta R}\right) \int_0^\infty [F(k) + F(-k)] \cos [kx - \Omega(k)t]dk$$

$$+ \sin\left(\frac{t}{\delta R}\right) \int_0^\infty [F(k) - F(-k)] \sin [kx - \Omega(k)t]dk \qquad (6.1a)$$

where

$$\Omega(k) = \frac{(\gamma - 1)k}{\delta(K_2 + \gamma K_1)} . \qquad (6.1b)$$

The "rapid" 6 day period oscillation comes from the terms $\cos (t/\delta R)$ and $\sin (t/\delta R)$. The packets arise from the Fourier inversion of terms involving $\cos [kx - \Omega(k)t]$ and $\sin [kx - \Omega(k)t]$. Phase modulation occurs because the frequency Ω depends on k. The period of the primary wave packet at $x = 10$ is approximately 50 days and the period of subsequent wave packets is approximately 24 days. Notice that the 6 day rapid oscillation remains unchanged as time evolves. It is interesting to note that $\Omega(k)$ is identical in form to the frequency $\omega(k)$ in the study of Mysak (1969). However, the parameter γ in the Mysak (1969) study is simply the ratio of the depth on the deeper side to that on the shallow side of the escarpment, and is consequently larger than the value of γ in this study. Therefore $\Omega(k)$ can be interpreted as the equivalent frequency for a homogeneous system with a small step.

Eqs. (3.9) can be used to calculate the flow field in each layer on either side of the step. The wavelength exhibited by the primary internal double Kelvin wave is of the order of 200 km. If this wave propagated as a free wave then the associated flow field would be near barotropic (see Section 4). However, free waves with wavelength shorter than $r_{i2}^{(S)}$ will become increasingly confined to the lower layer. Using (3.9), the velocity components are calculated during the first 25 units of time after the forcing is applied, to examine the distribution of the flow field within the two layers. In Figure 10 the velocity vectors in the upper and lower layers along the lines $y = \pm 0.1$ are plotted with time as a parameter. The velocity calculations are performed close to the step because the flow field will decay exponentially with increasing distance measured normal to the escarpment. Points closer to the escarpment will have larger velocities. From an examination of (3.9) it is clear that if all partial derivatives of ψ and η_2 are order one quantities, then the velocity components will be small. This is confirmed by the numerical evaluation of (3.9). For the Mendocino escarpment parameters, the scaling factor $\tau_0/(\rho_1\sigma_0 H_1)$ for the velocity components is 12.8 cm s^{-1}.

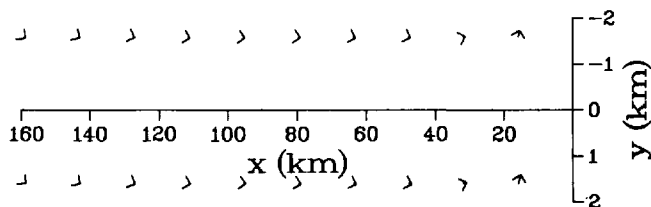The following observations should be noted about the velocity vectors in Figure 10:

(i) the velocity component normal to the step is larger than that parallel to the step in both layers.

(ii) as $x \rightarrow \infty$ the velocity field decays to zero in each layer.

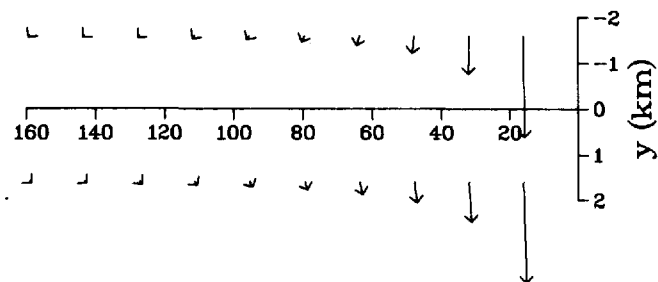# Time = 12.35 Days

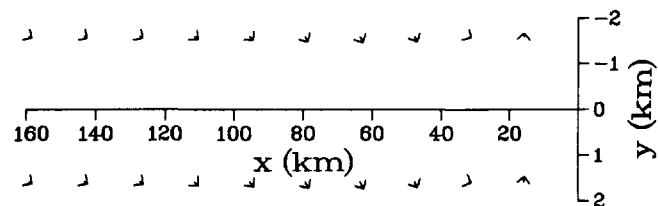## Upper Layer Velocities
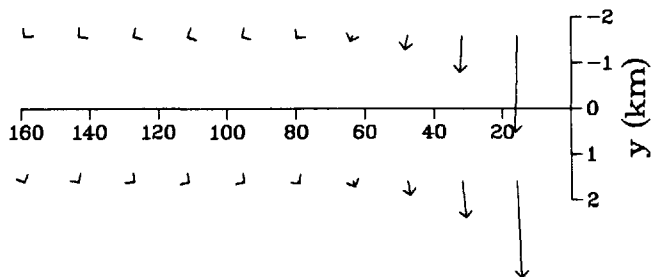
Lower Layer Velocities

Time = 37.06 Days

Upper Layer Velocities

Lower Layer Velocities

Time = 61.76 Days

Upper Layer Velocities

Lower Layer Velocities

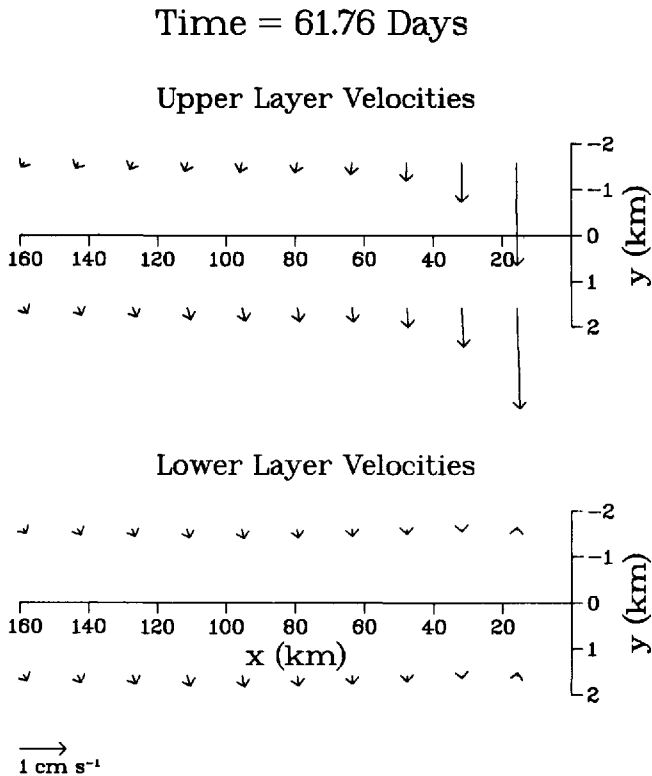$$\xrightarrow{}$$
1 cm s⁻¹

Figure 10. Velocity vectors in the upper and lower layers along $y = \pm 0.1$ and $x = 1, 2, \ldots, 10$ with dimensionless time as a parameter; (a) $t = 5$, (b) $t = 15$, (c) $t = 25$.

(iii) at the times displayed, the largest velocities occur within one Rossby radius of the wind stress curl origin and are produced by the permanently upwelled interface. The maximum velocity in Figure 10 is approximately 2 cm s⁻¹.

(iv) on the equatorward side of the step the upper layer velocities are larger than those in the lower layer in a region which increases in size at the rate of the phase speed of the primary wave. Ahead of this region the lower layer velocities exceed those in the upper layer.

(v) on the poleward side of the escarpment the upper layer velocities also exceed those in the lower layer within the first 5 to 6 units measured in the positive x-direction. This region does not appear to propagate.

(vi) in general, the velocity component parallel to the escarpment is directed in the positive x-direction on the poleward side of the step, while that on the equatorward side is directed in the negative x-direction. In terms of the Mendocino escarpment, the flow on the equatorward side will therefore tend to

be *equatorward* and *onshore*, while that on the poleward side of the step will also be equatorward and *offshore*. It must be stressed that these flow field directions occur within the first 25 units (60 days) after the wind stress is applied.

(vii) the departure from lower layer intensification is a consequence of the propagation characteristics of the forced wave and the steady state response.

Experiment 2. In this case, the only parameter altered from Experiment 1 is the *e*-folding time scale of the wind stress. A value of 1.2 days is assigned to σ_0^{-1}, thereby producing a more rapid decay of the wind stress than in the previous case. Notice in Experiment 1 that the work done by the wind stress goes into permanently upwelling the interface, generating Kelvin waves and exciting a transient response. If the wind stress decays more rapidly the work done by the stress on the ocean will be less and therefore the steady state upwelling response should be smaller. This is confirmed numerically.

The two important results found in this case are (a) slightly smaller wave amplitudes are generated because less work is done by the wind stress on the ocean and (b) the time period of the oscillations of $\partial\eta_2/\partial x$ and η_2 about the axis of zero displacement, as well as the wave packet periods, remain unaltered. Figure 11 clearly supports conclusion (b) by displaying $\partial\eta_2/\partial x$ as a function of time at $x = 2$ and $x = 10$. In fact, provided that the layer depths remain fixed the temporal variability of the waves is independent of the time scale of the transient wind stress (see (6.1)).

The reduction of the work done by the wind stress on the ocean compared with Experiment 1 also manifests itself in the steady state response. Figure 12 displays the steady state contribution to both $\partial\eta_2/\partial x$ and η_2 and shows a greatly diminished response compared with the corresponding figure in Experiment 1. Qualitatively the evolution in time of the wave part of η_2 is identical to that displayed in Figures 7 and 8 and therefore no plots will be displayed. However the phase speed of the primary wave in the early stages of development (the first 12 days after the wind stress is applied) is approximately 5 km day^{-1}. The total interfacial excursion is approximately two thirds of that in Experiment 1—namely 4 m.

Experiment 3. Additional numerical calculations are not required if reduced gravity is altered because this quantity does not appear in the inversion integral. The effect on the solutions of increasing the value of g' to 2×10^{-2} m s^{-2} can be seen in Table 1. As expected the scale parameter of the interfacial displacement is reduced (because increased buoyancy inhibits vertical motion) when g' is increased. Furthermore a corresponding increase in the horizontal length scale occurs. Therefore if the solutions in Experiment 1 are reanalyzed when $g' = 2 \times 10^{-2}$ m s^{-2}, the amplitude of the response will be halved and the wavelength along the step will be doubled.
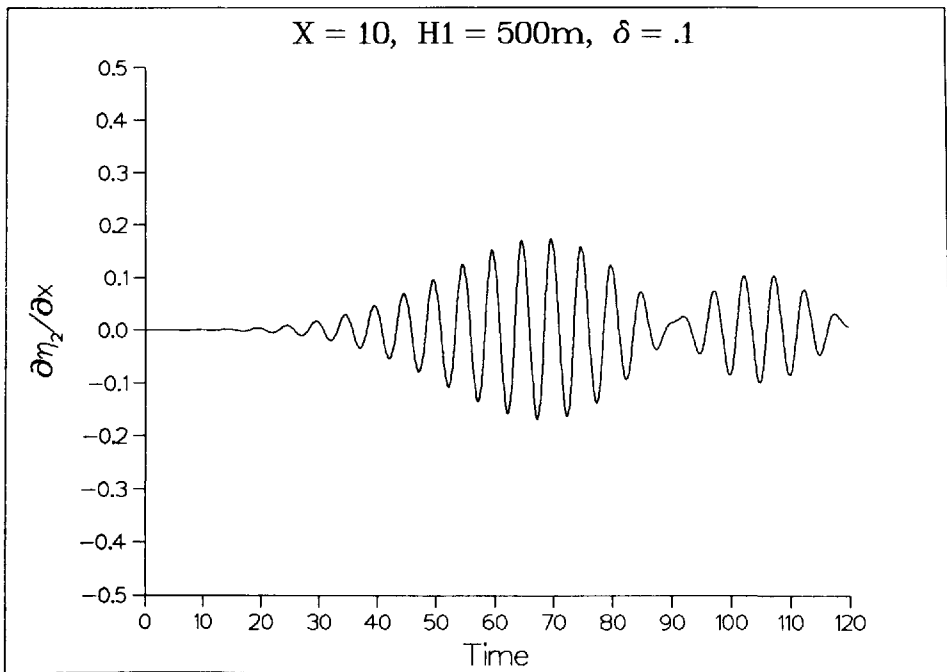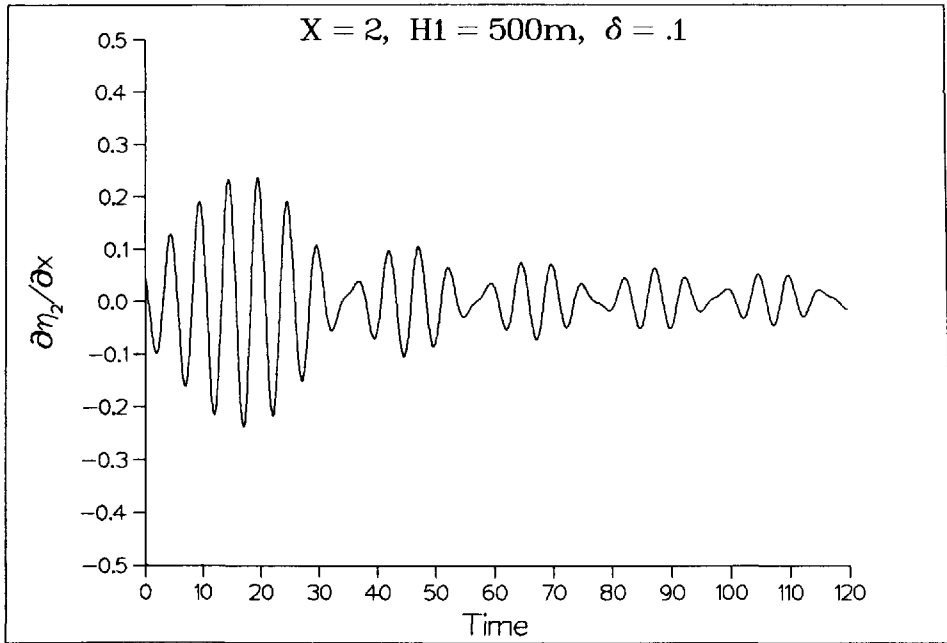
Figure 11. As in Figure 9, except the parameter values chosen are given in Table 1 under Experiment 2.
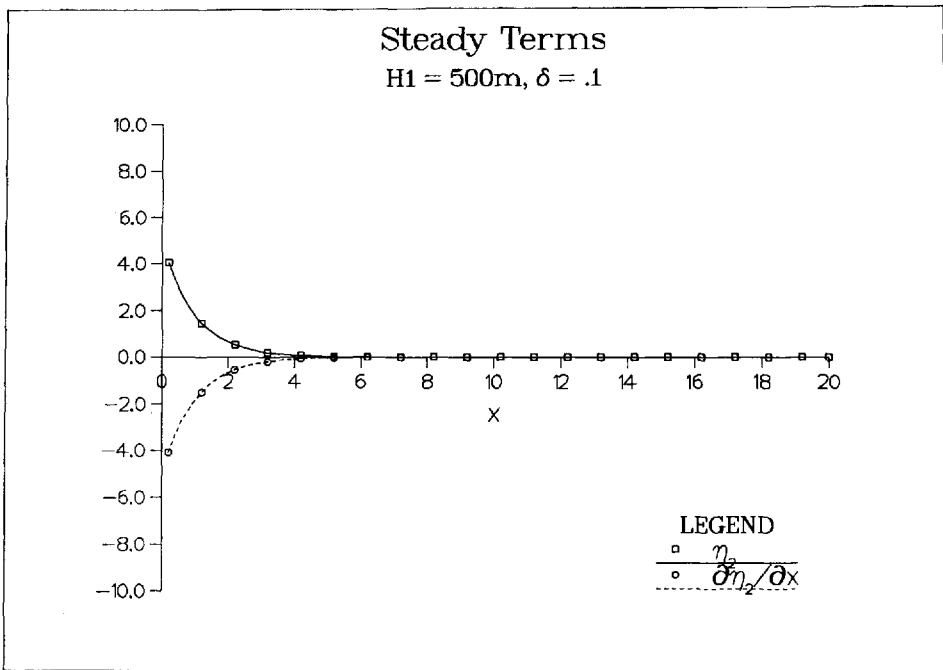
Figure 12. As in Figure 6, except the parameter values chosen are given in Table 1 under Experiment 2.

Experiment 4. In this case the fundamental parameter values employed in Experiment 1 are used, with the exception of the upper layer depth H_1, which is reduced to 100 m. Although this upper layer depth is too shallow for typical stratification found over the Mendocino escarpment, it is nevertheless instructive to examine the forced response for a range of layer depths.

The steady state contribution to η_2 plotted as a function of x is identical to Figure 6. However, since the scaling factor for the interfacial displacement η_0 is now 4.27 m, the amplitude of the steady state response ranges from 35.5 m at $x = 0$ to almost zero at a distance of 44.4 km from the origin.

Once again the wave contribution to η_2 evolves in time in a manner identical to the previous cases. The maximum interfacial excursion is now only 2 m and the phase speed of the primary wave is reduced to 0.13 km day^{-1}. In Figure 13 the temporal behavior of $\partial \eta_2/\partial x$ at $x = 2$ and $x = 10$ is displayed. At $x = 2$ the period of the oscillations is 6 days and the primary wave packet has a period in excess of 240 days. The slow growth of the primary wave packet in Figure 13b is consistent with the greatly reduced phase speed.

Experiment 5. All parameter values prescribed are identical to the previous case with the exception of g' which has a value of 2×10^{-2} m s^{-2}. Table 1 shows the
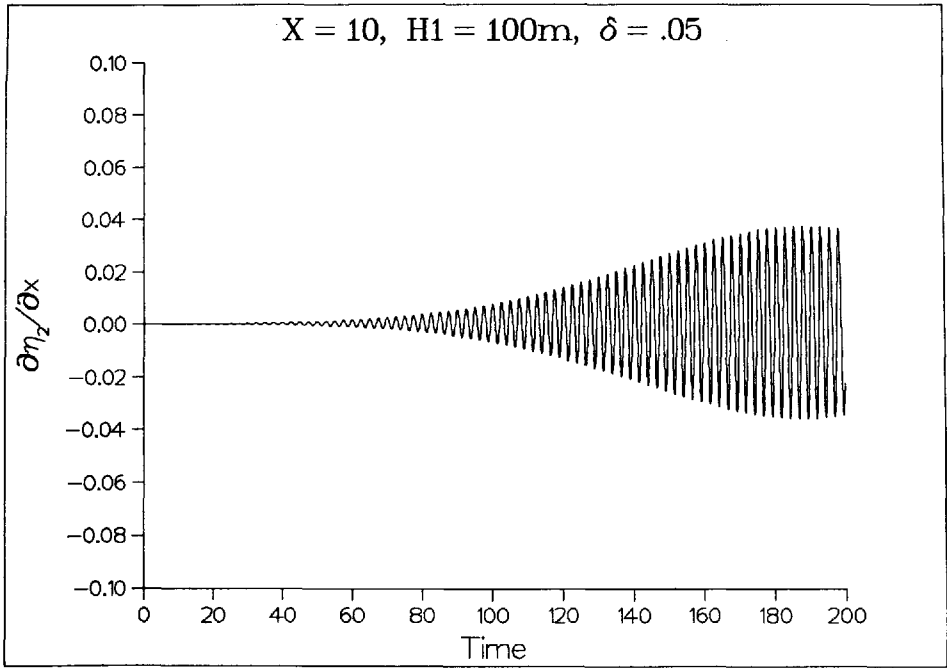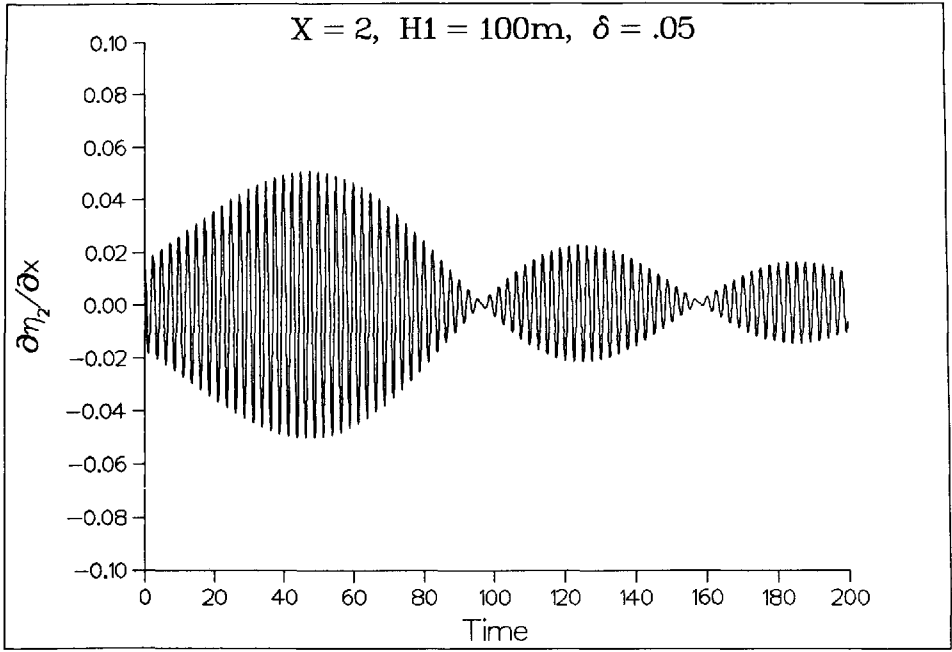
Figure 13. As in Figure 9, except the parameter values chosen are given in Table 1 under Experiment 4.

characteristic length scale (internal Rossby radius) increases to 14.2 km while the scale factor for the interfacial displacement is reduced to 2.13 m. This results in unreasonably small amplitude waves which would be impossible to detect in an ocean environment and therefore no further discussion will be presented for this case.

7. Response to a time-periodic wind stress

In this section the dependence of the Kelvin wave response with the wind stress orientation is considered. To simplify the analysis the wind stress chosen is spatially constant.

The first example presented in this section examines the Kelvin wave response generated by a time-periodic wind stress directed parallel to the escarpment. Following the method outlined in Section 5, it is found that when

$$\tau^x = -\tau_0 H(t) \cos(\sigma_0 t), \quad \tau^y = 0$$

the nondimensional interfacial displacement is given by

$$\eta_2(t) = \frac{(\gamma - 1)R}{2\pi(\gamma^{1/2} + \gamma)(1 - \delta^2 R^2)} \left[\sin\left(\frac{t}{\delta R}\right) - \delta R \sin t \right]. \tag{7.1}$$

Solution (7.1) exhibits the following important properties:

(i) a resonant response occurs when $\delta = R^{-1}$. For typical Mendocino escarpment parameters resonance occurs when $\delta \simeq 0.125$ which corresponds to a wind stress period of approximately 6.2 days. As $\delta R \to 1$ the solution (7.1) in fact becomes

$$\eta_2(t) = \frac{(\gamma - 1)R}{4\pi(\gamma^{1/2} + \gamma)} [t \cos t + \sin t]$$

and grows linearly with time.

(ii) The interfacial displacement does not have a travelling wave form.

(iii) Two periods are exhibited by η_2. The second term on the right-hand side of (7.1) exhibits the period of the wind stress forcing, while the first term exhibits the period of a freely propagating internal double Kelvin wave of infinitely long wavelength (see Section 4).

In the second example the wind stress is now rotated counterclockwise through 90° so that

$$\tau^x = 0, \quad \tau^y = -\tau_0 H(t) \cos(\sigma_0 t).$$

For this case the dimensionless interfacial displacement becomes

$$\eta_2(t) = \frac{1}{2\pi} \frac{(\gamma - 1)}{(\gamma^{1/2} + \gamma)} [1 - \cos t]. \tag{7.2}$$

The most striking difference between (7.2) and (7.1) is that the former does not exhibit resonance. Only the forcing period appears in (7.2). The absence of the internal Kelvin wave oscillation can be explained in terms of wind-driven Ekman transport. When the spatially constant stress is directed normal to the escarpment the mass transport is parallel to the step and therefore there is no wave generating mechanism.

8. Concluding remarks

A model for a two-layer uniformly rotating ocean of infinite horizontal extent in the presence of a step discontinuity in depth subject to a divergence-free wind stress applied normal to the escarpment, is presented. The response of the interface consists of the superposition of steady state, transient and wavelike terms when a wind stress curl of delta function form is applied. For parameter values suitable for the Mendocino escarpment it is found that the wavelike contribution to the solution for the interfacial displacement can exhibit a 6 m vertical excursion. The 6 m vertical excursion is obtained when a 500 m upper layer depth is chosen. A deeper upper layer will produce larger vertical excursions. Furthermore the 6 m vertical excursion occurs 80 km along the escarpment (in the direction of phase propagation) from the point where the delta function wind stress curl operates. Qualitatively the double Kelvin wave response resembles the forced external wave solutions obtained by Mysak (1969). However the wavelength of the primary forced wave obtained in this study is of the order of 200 km, rather than 10^4 km obtained by Mysak (1969) for the homogeneous model.

Wind stress orientation is also addressed in this study by examining the response produced by a spatially independent time-periodic stress aligned either normal or parallel to the escarpment. In each case travelling waves are not generated. When the stress is directed parallel to the escarpment resonance can occur at parameter values which are not unreasonable for the Mendocino escarpment region (wind stress period of 6.2 days). The interface oscillates harmonically in time with two periods; the forcing period and the barotropic double Kelvin wave period. Rotating the same wind stress through 90° produces a response in which the Kelvin wave term is absent. All the wind stresses prescribed in this paper have no intrinsic length scale. The solutions obtained therefore exhibit, in some sense, the natural length scale for the problem.

This study suggests that approximately one month after the sudden intensification and subsequent decay of a large anticyclonic weather system along the central California coast, a measurable displacement of the isotherms within the pycnocline will occur as the primary forced double Kelvin wave propagates along the escarpment. The detection of internal double Kelvin waves should be possible. An ideal data base to use would be a one year time series of isotherm displacements within the thermocline at various locations over the escarpment. The theoretical 6 day oscillation should be a dominant signal in any spectra computed from such a record. Of course, the ocean response will be complicated because over a one month period, more than one storm

event can occur, which will give rise to the superposition of forced waves generated at different locations and times over the escarpment.

Further studies of forced waves over oceanic escarpments are clearly required because the model presented here is deficient in three important areas. Firstly, the presence of the California coast (a boundary normal to the escarpment) has been neglected. A future study will report on the generation of double Kelvin waves in a homogeneous ocean along a semi-infinite escarpment. The inclusion of stratification in a linear forced wave model with a semi-infinite escarpment presents a challenging problem, which will probably require a numerical approach. As an aid to understanding the low frequency variability of the California Current System this problem should be addressed however.

The second problem with the model presented here is the approximation of the Mendocino escarpment by a step. A seascarp with a continuous and monotonic depth profile which is asymptotic to the uniform depths $H_1 + H_2^{(N)}$ and $H_1 + H_2^{(S)}$ would be more realistic. Longuet-Higgins (1968b) has considered trapped free waves over such an escarpment. In Figure 2 the presence of large seamounts located along the escarpment are observed. Seamounts will tend to scatter energy associated with trapped waves over the escarpment, thereby reducing the effectiveness of this natural oceanic waveguide.

Finally Chapman (1982) has conducted an extensive comparison of trapped free wave dispersion properties over a discontinuity in depth in a homogeneous ocean and a continuously stratified ocean. Only at the long wavelength, low frequency limit does the homogeneous model predict dispersion characteristics that are in agreement with those exhibited by the continuously stratified model. Chapman (1982) also finds that even at the long wavelength, low frequency limit of the free waves the phase and group velocities differ substantially between the two models. As yet a comparison between the unforced internal double Kelvin wave solution in a two-layer model with the unforced baroclinic waves in a continuously stratified ocean over a depth discontinuity remains to be made. Furthermore the differences in the propagation characteristics of forced trapped (or leaky) wave solutions in homogeneous, discrete density layered and continuously stratified oceans is still open to debate. It seems reasonably safe to say that in the light of the study by Chapman (1982), the magnitude of the phase speeds predicted by the model presented in this paper will differ by as much as 40% from the corresponding phase speed in an ocean with continuous (realistic) stratification.

APPENDIX A

Derivation of the free-wave dispersion relation

The derivation of the dispersion relation follows the method described by Wright and Mysak (1977) for obtaining the dispersion relation for long coastal trapped waves of subinertial frequency over a single-step continental shelf in a two-layer fluid.

In the absence of wind stress forcing, the dependent variables in (2.1) to (2.6) are written in the form $\zeta(x, y, t) = Re\{\zeta(x, y)e^{-i\omega t}\}$. Expressions analogous to (2.9) for u_1, v_1 and u_2, v_2 in terms of η_1 and η_2 are then obtained in the manner described in Section 2. These equations are used in deriving the governing equation for η_2 and in the matching conditions across the escarpment.

The equations analogous to (2.12) and (2.14) are

$$\nabla^2\psi = 0, \tag{A1}$$

and

$$\nabla^2\eta_2 - \frac{1}{r_{i2}{}^2}\eta_2 = 0, \tag{A2}$$

and are obtained following the approach described in Section 2. However, in (A1) and (A2) the quantities ψ and η_2 are functions of x and y only.

At the escarpment $y = 0$, the continuity of the sea surface and interfacial displacement requires

$$\left.\begin{aligned} -i\omega u_1{}^{(N)} - fv_1{}^{(N)} &= -i\omega u_1{}^{(S)} - fv_1{}^{(S)}, \\ \eta_2{}^{(N)} &= \eta_2{}^{(S)}, \end{aligned}\right\} \text{ at } y = 0. \tag{A3a} \tag{A3b}$$

The mass transport normal to the escarpment is also continuous in each layer, and therefore

$$\left.\begin{aligned} v_1{}^{(N)} &= v_1{}^{(S)}, \\ H_2{}^{(N)}v_2{}^{(N)} &= H_2{}^{(S)}v_2{}^{(S)}, \end{aligned}\right\} \text{ at } y = 0. \tag{A4a} \tag{A4b}$$

Upon combining Eqs. (A4a, b) it is clear that

$$\psi_x{}^{(N)} = \psi_x{}^{(S)} \text{ at } y = 0. \tag{A5}$$

For trapped waves that propagate along the escarpment, solutions of the form

$$\left.\begin{aligned} \psi(x, y) &= \Phi(y)e^{ikx}, \\ \eta_2(x, y) &= H(y)e^{ikx}, \end{aligned}\right\} k > 0 \tag{A6} \tag{A7}$$

are examined. When (A6) and (A7) are substituted into (A1) and (A2) respectively, it

is found that

$$\Phi_{yy} - k^2\Phi = 0, \tag{A8}$$

$$H_{yy} - \lambda^2 H = 0, \tag{A9}$$

where $\lambda^2 = k^2 + 1/r_{i2}^2$. Upon solving (A8) and (A9) and applying the trapping condition, (A5) and (A3b), it is found that

$$\psi^{(N)} = A_1 e^{|k|y} e^{ikx}, \tag{A10a}$$

$$\psi^{(S)} = A_1 e^{-|k|y} e^{ikx}, \tag{A10b}$$

$$\eta_2^{(N)} = A_2 \exp(\lambda^{(N)}y) \exp(ikx), \tag{A11a}$$

$$\eta_2^{(S)} = A_2 \exp(-\lambda^{(S)}y) \exp(ikx), \tag{A11b}$$

where $\lambda^{(N)} = (k^2 + 1/r_{i2}^{(N)2})^{1/2}$, $\lambda^{(S)} = (k^2 + 1/r_{i2}^{(S)2})^{1/2}$ and A_1, A_2 are arbitrary constants. Finally, the application of (A3a) and (A4b), using (A10) and (A11), gives two homogeneous equations for A_1 and A_2, namely

$$A_1 + \frac{g'A_2}{f^2}\left\{fH_1 + \frac{\omega}{k(H_2^{(S)} - H_2^{(N)})}[H_2^{(N)}H^{(S)}\lambda^{(N)} + H_2^{(S)}H^{(N)}\lambda^{(S)}]\right\} = 0, \tag{A12}$$

$$A_1 + \frac{g'H_1(H_2^{(S)} - H_2^{(N)})A_2}{[\omega(H^{(S)} + H^{(N)}) + f(H_2^{(S)} - H_2^{(N)})]} = 0. \tag{A13}$$

Upon setting the determinant of the coefficients of (A12) and (A13) to zero, the dispersion relation (4.1) is obtained.

APPENDIX B

Numerical evaluation of Fourier integrals

The inversion of the expression $i k \tilde{\eta}_2(k, 0, t)$ which appears in Section 5 gives rise to Fourier integrals of the type

$$I(x, t) = \int_0^\infty f(k, t) \begin{vmatrix} \cos \\ \sin \end{vmatrix} (kx)\, dk. \tag{B1}$$

Integrals of the type (B1) are difficult to evaluate accurately because (a) for large k the integrand oscillates rapidly thereby producing extremely strong cancellation of the positive and negative contributions to I and (b) when f decays slowly to zero as $k \to \infty$ the problem stated in (a) is accentuated. Blakemore *et al.* (1976) discuss a number of related methods for the evaluation of (B1). The approach adopted in this paper is to integrate between successive zeros of $\cos(kx)$ (or $\sin(kx)$), thus converting the integral (B1) to an infinite summation. Following Blakemore *et al.* (1976) it can be shown that if

$$I_c(x, t) = \int_0^\infty f(k, t) \cos(kx)\, dk, \tag{B2}$$

then (B2) may be expressed as

$$I_c(x, t) = x^{-1} \int_0^{\pi/2} f(p/x, t) \cos p \, dp + \sum_{n-0}^{\infty} u_n(x, t),$$ (B3)

where

$$u_n(x, t) = (-1)^{n+1} x^{-1} \int_0^{\pi} f[(p + n\pi + \pi/2)x^{-1}, t] \sin p \, dp.$$ (B4)

Similarly, if

$$I_s(x, t) = \int_0^{\infty} f(k, t) \sin(kx) \, dk,$$ (B5)

then (B5) may be expressed as

$$I_s(x, t) = \sum_{n-0}^{\infty} v_n(x, t)$$ (B6)

where

$$v_n(x, t) = (-1)^n x^{-1} \int_0^{\pi} f[(p + n\pi)x^{-1}, t] \sin p \, dp.$$ (B7)

The finite range integrals appearing in (B3), (B4) and (B7) are evaluated using a cautious adaptive Romberg extrapolation scheme. To accelerate the convergence of the alternating infinite series appearing in (B3) and (B6) a variation of the Shanks transform technique is employed (see Shanks, 1955). Blakemore *et al.* (1976) discuss a number of accelerator techniques for the evaluation of slowly converging alternating infinite series. The basic idea of these algorithms is to accelerate the convergence of the sequences $\{A_n\}$ ($n = 0, 1, 2, \ldots$) of partial sums given by

$$A_n = \sum_{j-0}^{n} u_j$$

In this paper the accelerator chosen is the numerically stable ϵ-algorithm (see Blakemore *et al.*, 1976) defined by

$$\left. \begin{array}{l} \epsilon_n^{(-1)} = 0; \quad \epsilon_n^{(0)} = A_n \\ \epsilon_n^{(p)} = \epsilon_{n+1}^{(p-2)} + [\epsilon_{n+1}^{(p-1)} - \epsilon_n^{(p-1)}]^{-1} \end{array} \right\}$$ (B8)

The recurrence relations defined in (B8) are used to calculate $\epsilon_0^{(2k)}$ ($k = 1, 2, \ldots$). For fixed k, the first $(2k + 1)$ partial sums are required to calculate $\epsilon_0^{(2k)}$. Furthermore the value of $\epsilon_0^{(2k)}$ is a more accurate approximation to the value of the sum of the altering infinite series than A_{2k+1}. The integrals in Section 5 are approximated by the value of $\epsilon_0^{(10)}$ (corresponding to a value of $k = 5$).

REFERENCES

Allen, J. S. 1975. Coastal trapped waves in a stratified ocean. J. Phys. Oceanogr., *5*, 300–325.

Blakemore, M., G. A. Evans and J. Hyslop. 1976. Comparison of some methods for evaluating infinite range oscillatory integrals. J. Comput. Phys., *22*, 352–376.

Chapman, D. C. 1982. On the failure of Laplace's tidal equations to model subinertial motions at a discontinuity in depth. Dyn. Atmos. Oceans, *7*, 1–16.

Clarke, A. J. 1977. Wind-forced linear and nonlinear Kelvin waves along an irregular coastline. J. Fluid Mech., *83*, 337–348.

LeBlond, P. H. and L. A. Mysak. 1978. Waves in the Ocean. Elsevier, 602 pp.

Lighthill, M. J. 1958. Fourier Analysis and Generalised Functions. Cambridge Univ. Press, 79 pp.

Longuet-Higgins, M. S. 1968a. On the trapping of waves along a discontinuity of depth in a rotating ocean. J. Fluid Mech., *31*, 417–434.

—— 1968b. Double Kelvin waves with continuous depth profiles. J. Fluid Mech., *34*, 49–80.

Mysak, L. A. 1969. On the generation of double Kelvin waves. J. Fluid Mech., *37*, 417–434.

—— 1977. On the stability of the California Undercurrent off Vancouver Island. J. Phys. Oceanogr., *7*, 904–917.

Rhines, P. B. 1977. The dynamics of unsteady currents, *in* The Sea, E. D. Goldberg *et al.*, eds., *6*, Wiley (Interscience), New York, 189–318.

Shanks, D. 1955. Non-linear transformations of divergent and slowly convergent sequences. J. Math and Phys., *34*, 1–42.

Wright, D. G. and L. A. Mysak. 1977. Coastal trapped waves, with application to the Northeast Pacific Ocean. Atmosphere, *15*, 141–150.